

Forming spectroscopic massive proto-binaries by disk fragmentation

D. M.-A. Meyer,^{1*} R. Kuiper,¹ W. Kley,¹ K. G. Johnston² and E. Vorobyov^{3,4,5}

¹*Institut für Astronomie und Astrophysik, Universität Tübingen, Auf der Morgenstelle 10, 72076 Tübingen, Germany*

²*School of Physics and Astronomy, E.C. Stoner Building, The University of Leeds, Leeds LS2 9JT, UK*

³*Institute of Fluid Mechanics and Heat Transfer, TU Wien, Vienna, 1060, Austria*

⁴*Department of Astrophysics, The University of Vienna, Vienna, A-1180, Austria*

⁵*Research Institute of Physics, Southern Federal University, Stachki 194, Rostov-on-Don, 344090, Russia*

Received Month Day Year; accepted Month Day Year

ABSTRACT

The surroundings of massive protostars constitute an accretion disc which has numerically been shown to be subject to fragmentation and responsible for luminous accretion-driven outbursts. Moreover, it is suspected to produce close binary companions which will later strongly influence the star's future evolution in the Hertzsprung-Russel diagram. We present three-dimensional gravitation-radiation-hydrodynamic numerical simulations of 100 M_{\odot} pre-stellar cores. We find that accretion discs of young massive stars violently fragment without preventing the (highly variable) accretion of gaseous clumps onto the protostars. While acquiring the characteristics of a nascent low-mass companion, some disc fragments migrate onto the central massive protostar with dynamical properties showing that its final Keplerian orbit is close enough to constitute a close massive proto-binary system, having a young high-mass and a low-mass component. We conclude on the viability of the disc fragmentation channel for the formation of such short-period binaries, and that both processes – close massive binary formation and accretion bursts – may happen at the same time. FU-Orionis-type bursts, such as observed in the young high-mass star S255IR-NIRS3, may not only indicate ongoing disc fragmentation, but also be considered as a tracer for the formation of close massive binaries – progenitors of the subsequent massive spectroscopic binaries – once the high-mass component of the system will enter the main-sequence phase of its evolution. Finally, we investigate the ALMA-observability of the disc fragments.

Key words: stars: protostars – accretion discs – stars: massive – methods: numerical

1 INTRODUCTION

Massive star formation is a process happening in large, cold and opaque molecular clouds (Zinnecker & Yorke 2007; Langer 2012) but its repercussions upon the functioning of the interstellar medium are huge (Vink 2006, 2012). Understanding the formation of these high-mass stars in detail would allow us to predict – given a set of initial properties of the parent molecular cloud in which these stars form – their final fate, e.g. as core-collapse supernovae or gamma-ray bursts (Woosley et al. 2002). It has been shown that most of the massive stars experience (close) multiplicity even during their early main-sequence phase (Vanbeveren 1991; Mahy et al. 2013), which in turn strongly impacts their future evolutionary path in the Hertzsprung-Russel diagram (Dessart et al. 2003; Petrović 2004; Sana et al. 2012). Additionally, while rapidly leaving their pre-main-sequence tracks, high accretion rates of circumstellar material $\sim 10^{-3} M_{\odot} \text{ yr}^{-1}$ can already affect the evolution of massive

protostars before entering the main-sequence phase (Hosokawa & Omukai 2009; Haemmerlé et al. 2016, 2017).

Close massive binaries are believed to have formed in the surroundings of pre-main-sequence massive stars, by analogy with low-mass star formation (Bonnell & Bate 1994). Consequently, the detailed study of the proto-circumstellar medium of young high-mass stars is a preponderant step towards a complete stellar evolution of massive stars. Amongst the several formation scenarios of massive binaries that have been proposed, the direct formation of low-mass companion(s) from the fragmentation of the accretion disc of a still growing massive protostar is one of the most natural (Cesaroni et al. 2006). It consists in assuming that high-mass star formation is a scaled-up version of the formation of low-mass stellar systems (Fuente et al. 2001; Testi 2003) and the formation of companions to massive stars might be seen as a scaled up version of gas giant planet formation via gravitational instability. This is strengthened by more and more unambiguous observations of collapsing high-mass pre-stellar cores (Beuther et al. 2015), jets (Purser et al. 2016) and accretion flows at their center (Keto & Wood 2006). Several circumstellar mechanisms asso-

* E-mail: dominique.meyer@uni-tuebingen.de

ciated to disc accretion have been observed, such as ionized HII regions channeled into cavities shaped by bipolar outflows (Cesaroni et al. 2010).

Direct imaging of discs are only beginning to be resolvable by modern facilities (Beuther et al. 2012). Particularly, the *Atacama Large (sub-)Millimeter Array (ALMA)* recently revealed the existence of a Keplerian accretion disc around the forming O-type star AFL 4176 (Johnston et al. 2015) and in the surroundings of the young early massive star G11.920.61 MM1 (Ilee et al. 2016). More recently, observations of the high-mass proto-binary IRAS17216-3801 in Kraus et al. (2017) revealed together the circumstellar accretion discs of each massive components of a system similar to the numerical model of Krumholz et al. (2009a), themselves surrounded by a circumbinary disc.

The physics of collapsing gaseous clouds has been extensively studied (Evans 1999; Bergin & Tafalla 2007; McKee & Ostriker 2007, and references therein), and angular momentum conservation may lead to the formation of an accretion disc. Many mechanisms have been proposed to explain angular momentum transport in accretion discs around low-mass stars such as baroclinic instabilities (Klahr & Bodenheimer 2003; Klahr 2004), convective instabilities (Lin et al. 1993), magneto-rotational instabilities (Ruden & Pollack 1991; Hawley & Balbus 1992; Flaig et al. 2012) and vertical shear instabilities (Nelson et al. 2013; Stoll & Kley 2014). Nonetheless, gravitational torques arising from the innermost to the outer part of self-gravitational discs is the most efficient momentum transport phenomenon in discs around high-mass stars (Kuiper et al. 2011). After the gravitational collapse of pre-stellar cores, spiral arms developing in accretion discs may become unstable and experience local gravitational collapse leading to the formation of dense gaseous clumps - progenitors of massive giant planets, brown dwarfs or stellar companions (Stamatellos & Whitworth 2009a; Vorobyov 2013; Boss 2017). The migration of disc substructures (clumps, spiral arcs) onto their central protostar is responsible for violent accretion-driven outbursts broadly studied in the low-mass (Vorobyov 2010), the high-mass (Meyer et al. 2017) and the primordial (Vorobyov 2013; Hosokawa et al. 2016) regimes of star formation.

The surroundings of young stars has been investigated with sophisticated numerical models including appropriate physical processes such as the presence of the cloud magnetic fields (Banerjee et al. 2004; Banerjee & Pudritz 2006; Commerçon et al. 2010; Fendt 2011; Fendt & Shekhnazami 2013; Machida & Hosokawa 2013; Seifried et al. 2013; Stepanovs et al. 2014; Seifried et al. 2015) or (external) stellar radiation feedback (Yorke & Welz 1996; Richling & Yorke 1997; Kessel et al. 1998; Richling & Yorke 1998, 2000). However, only a small number of studies tackled the problem of star formation in its high-mass regime (Bonnell et al. 1998; Yorke & Sonnhalter 2002; Banerjee & Pudritz 2007; Krumholz et al. 2007b; Kuiper et al. 2010; Peters et al. 2010; Commerçon et al. 2011; Kuiper et al. 2011; Seifried et al. 2011, 2012; Kuiper et al. 2015; Harries 2015; Kuiper et al. 2016; Klassen et al. 2016; Harries et al. 2017). The outcomes of those studies have been post-processed with radiative transfer methods in order to obtain synthetic observations, e.g. as seen from the *ALMA* telescope (Krumholz et al. 2007a; Seifried et al. 2016). In addition to different spatial resolution that limits the proper capture of local gravitational collapse in a disc, those studies devoted to massive star formation differ by (i) the level of realism taken into account in order to model the proto-stellar feedback, (ii) the spatial resolution allowed by the scheme and (iii) the criteria applied to consider a dense region of the disc as a fragment, e.g. introducing sink parti-

cles (see Federrath et al. 2010, for a description of such technique).

The characterisation of the fragmentation of self-gravitating discs is not a trivial task and several criteria necessary but not sufficient have been derived so far. The coupling of N-body solvers to hydrodynamical codes via the introduction of sink particles alleviate the computation of longer timescales, because subgrid models save computing time since they do not have to resolve the smallest scales (Federrath et al. 2010). However, the required conditions of their creation throughout a simulation is subject to debate and may lead to artificial fragmentation which can, for instance, affects their host spiral arm dynamics. The two main of those criteria are the so-called Toomre and Gammie criteria and they compare the local effects of gravitational instability (Toomre 1963) and cooling (Gammie 1996) against the combined effects of the disc thermodynamics with the gas rotation shear, respectively. A large literature confronts these criteria with numerical simulations of protostellar and low-mass self-gravitating discs and highlights their sensitivity to initial conditions, viscosity, resolution and numerics (Stamatellos & Whitworth 2009b; Forgan et al. 2011; Lodato & Clarke 2011; Meru & Bate 2011; Forgan & Rice 2012; Rice et al. 2012; Paardekooper 2012; Rice et al. 2014; Tsukamoto et al. 2015). Interestingly, in Klassen et al. (2016), numerical simulations of massive protostellar discs that fulfill those criteria may not necessarily form fragments while this apparent stability is consistent with the so-called Hill criterion (Rogers & Wadsley 2012).

The consistency of a FU-Orionis-like scenario producing strong accretion outbursts by fast migration of disc debris has just been shown for massive star formation (Meyer et al. 2017) and is in accordance with the outflows observed in the young massive stellar system S255IR-SMA1 (Burns et al. 2016; Caratti o Garatti et al. 2016) and NGC6334I-MM1 (Hunter et al. 2017). In the present study, we extend our numerical investigation of the stability of self-gravitating accretion discs around massive protostars and its connection to the accretion-driven flares as well as multiplicity. While the scientific literature already covered the question of the gravitational collapse of massive ($\geq 30 M_{\odot}$) pre-stellar cores generating a massive protostar surrounded by a growing accretion disc, those studies generally assumed a simplified treatment of the protostellar feedback, i.e. within the flux-limited diffusion approximation (Krumholz et al. 2007b, 2009a) or suffer from a lack of resolution (Kuiper et al. 2011), especially in the region close to the star (Krumholz et al. 2007b, 2009a; Rosen et al. 2016; Klassen et al. 2016). The studies above presented evidence for (i) multiplicity in the high-mass regime by generating large-separation low-mass companions in spiral arms of massive protostellar accretion discs (Krumholz et al. 2007b; Rosen et al. 2016), (ii) massive binaries made of two high-mass protostars (Krumholz et al. 2009a), (iii) close massive binaries of two high-mass components (Bonnell & Bate 1994), while (iv) Klassen et al. (2016) does not conclude on the formation of stars around young massive protostellar objects. Nevertheless, no satisfactory theoretical models have yet explained the existence of small-separation/short-period low-mass companions to young high-mass stars. This is an important question because such systems are believed to evolve towards so-called spectroscopic (massive) binary systems, i.e. a particular class of close massive binaries made of an O-type star surrounded by one or more closely-separated low-mass companions (see Mahy et al. 2013; Kobulnicky et al. 2014).

The goal of this study consists in testing the disc fragmentation scenario for the formation of those short-period massive binaries made of a proto-O star and (at least) a close low-mass compan-

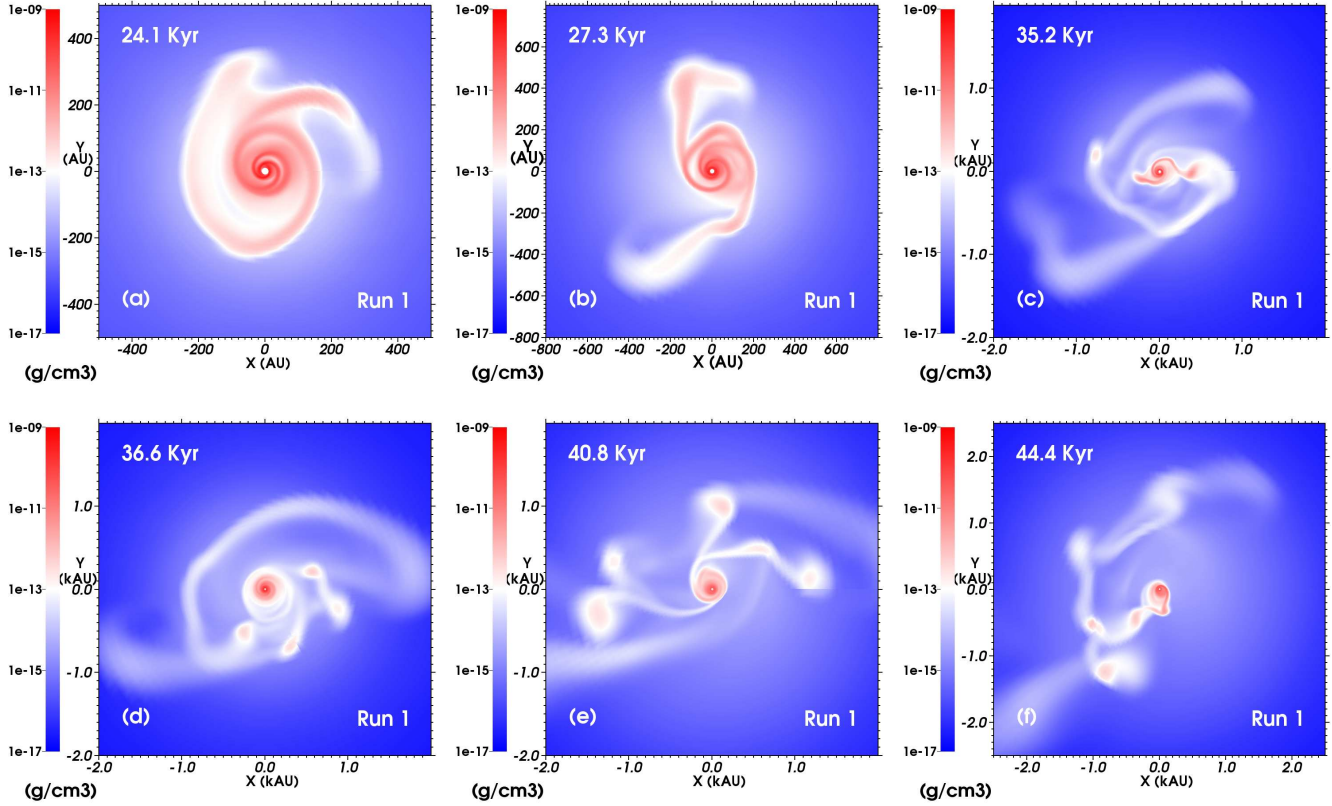


Figure 1. Midplane density (in g cm^{-3}) of the accretion disc generated in Run 1, showed at different characteristic times of its evolution (in kyr). The density is plotted on a logarithmic scale and the size of the panels is in AU (top left and middle panel) or kAU (elsewhere).

ion, using high-resolution hydrodynamical simulations of the gravitational collapse of rotating pre-stellar cores. We perform three-dimensional numerical simulations including self-gravity, radiative transport and a midplane-symmetric spherical computational domain centered at a sink cell in which a protostar is assumed to form and evolve. The young star acquires mass by disc accretion, as in many current studies devoted to disc fragmentation around low-mass and primordial protostars (Vorobyov & Basu 2007; Vorobyov et al. 2013; Vorobyov & Basu 2015; Hosokawa et al. 2016). Our highly-resolved models neglect the internal turbulence and magnetization of the collapsing pre-stellar cores but allow a sub-AU spatial resolution close to the protostar which is higher than in any models previously published so far. We find that all our modeled discs show clear sign of instability, fragment and generate a series of sudden increase of the accretion rate caused by fragments migrating towards the central protostar. Interestingly, some of those migrating clumps have interior thermodynamic properties indicating that they may be secondary pre-stellar embryos, and, therefore, we conclude on the viability of disc fragmentation as a channel for the formation of close low-mass companions to forming massive stars.

Our study is organized as follows. We begin in Section 2 with introducing the reader to our numerical setup. In Section 3, we describe our particular initial conditions in terms of density and angular frequency distribution of the collapsing pre-stellar cores that we consider. Their evolution, the formation of accretion discs and their subsequent fragmentation are qualitatively described in Section 4. In Section 5, we investigate the physical and numerical processes at work in this study, i.e. the role of the central protostellar irradiation

and the effects of the spatial resolution in the simulations, while we further test our outcomes for accretion disc against various criteria for disc stability in Section 6. In section 7 we detail the fate of the disc debris and investigate their properties as forming low-mass stars and further discuss our findings in the context of the formation of close massive binary systems. In Section 8 we compare our results to previous theoretical and observational studies. Finally, we give our conclusions in Section 9.

2 METHOD

In the following paragraphs, we introduce the reader to the method used to perform our numerical simulations. Our simulations model the collapse of a pre-stellar core forming around a self-gravitating accretion disc that evolves as being irradiated by the time-dependent luminosity of the central protostar. We detail the various assumptions and prescriptions used to model the microphysical processes of the gas and the dust of the pre-stellar core, describe the manner we treat the protostellar feedback onto the disc and we present the computational grid and the numerical scheme utilised in this study.

2.1 Governing equations

As other studies devoted to star formation, we work at the interplay between gas dynamics, gravity and radiation transport. The hydrodynamics is described by the equations of fluid dynamics for

Table 1. Initial conditions. Quantity β_Ω is the slope of the angular velocity index of the pre-stellar core. Simulations are run until t_{end} (in kyr).

Models	Angular frequency index β_Ω	t_{end} (kyr)	Motivation
Run 1	0.0	50.0	Solid-body rotation (cf. run M100 in Klassen et al. 2016)
Run 1-noIrr	0.0	45.0	cf. Run 1, without protostellar irradiation
Run 1-LR	0.0	40.0	cf. Run 1, with a coarser spatial resolution
Run 1-HR	0.0	32.1	cf. Run 1, with a finer spatial resolution
Run 2	-0.35	40.0	Intermediate initial angular velocity radial distribution
Run 3	-0.75	35.0	Steep initial angular velocity radial distribution (see Meyer et al. 2017)

compressible gas that consist of the relations for mass,

$$\frac{\partial \rho}{\partial t} + \nabla \cdot (\rho \mathbf{v}) = 0, \quad (1)$$

momentum,

$$\frac{\partial \rho \mathbf{v}}{\partial t} + \nabla \cdot (\rho \mathbf{v} \otimes \mathbf{v}) + \nabla p = \mathbf{f}, \quad (2)$$

and total energy conservation,

$$\frac{\partial E}{\partial t} + \nabla \cdot ((E + p)\mathbf{v}) = \mathbf{v} \cdot \mathbf{f} \quad (3)$$

where ρ , \mathbf{v} , p are the Eulerian variables, i.e. the mass density, the vector velocity and the gas pressure, respectively. The gas assumes an ideal equation of state $p = (\gamma - 1)E_{\text{int}}$ where $\gamma = 5/3$ is the constant adiabatic index. The variable E_{int} is the internal energy of the medium such that,

$$E = E_{\text{int}} + \frac{1}{2}\rho \mathbf{v}^2, \quad (4)$$

represents the total energy of the plasma.

The radiation transport scheme is taken from Kuiper et al. (2010). In Eqs. (2) and (3) the quantity,

$$\mathbf{f} = -\rho \nabla \Phi_{\text{tot}} - \frac{\rho \kappa_{\text{R}}(T_\star)}{c} \mathbf{F}_\star - \frac{\rho \kappa_{\text{R}}(T)}{c} \mathbf{F}, \quad (5)$$

is the force density vector with Φ_{tot} total gravitational potential, κ_{R} the Rossland opacity, c the speed of light, \mathbf{F} the radiation flux and \mathbf{F}_\star the stellar radiation flux. The equations of radiation transport govern the time-evolution of the radiation energy density E_{R} ,

$$\frac{\partial E_{\text{R}}}{\partial t} + f_{\text{c}} \nabla \cdot (\mathbf{F} + \mathbf{F}_\star) = 0, \quad (6)$$

where $f_{\text{c}} = 1/(c_{\text{v}}\rho/4aT^3 + 1)$ with c_{v} the specific heat capacity and a the radiation constant. We solve Eq. (6) in the flux-limited diffusion (FLD) approximation, where $\mathbf{F} = -D\nabla E_{\text{R}}$. The diffusion constant is $D = \lambda c/\rho \kappa_{\text{R}}$ where λ is the flux limiter and κ_{R} is the mean Rossland opacity. The relation,

$$\frac{\mathbf{F}_\star(r)}{\mathbf{F}_\star(R_\star)} = \left(\frac{R_\star}{r}\right)^2 e^{-\tau(r)}, \quad (7)$$

reports the decrease of the flux during the ray-tracing of the stellar incident radiation with the stellar radius R_\star and $\tau(r) = \kappa_{\text{P}}(T_\star)\rho(r)$ being the optical depth of the medium. The total opacity takes into account both the gas and the dust attenuation of the radiation, i.e., $\kappa_{\text{P}} = \kappa_{\text{P}}^{\text{g}} + \kappa_{\text{P}}^{\text{d}}$, where $\kappa_{\text{P}}^{\text{g}}$ and $\kappa_{\text{P}}^{\text{d}}$ are the gas and dust opacities, respectively. To this end, we use constant gas opacity of $\kappa_{\text{P}}^{\text{g}} = 0.01 \text{ cm}^2 \text{ g}^{-1}$ and utilise the tabulated dust opacity of Laor & Draine (1993). Gas and dust temperature are calculated assuming the equilibrium between the dust temperature and the to-

tal radiation field,

$$aT^4 = E_{\text{R}} + \frac{\kappa_{\text{P}}(T_\star)}{\kappa_{\text{P}}(T)} \frac{|\mathbf{F}_\star|}{c}. \quad (8)$$

We employed the time-dependent treatment of the dust for photoevaporation and sublimation described in Kuiper et al. (2011) and used in subsequent works (Hosokawa et al. 2016). At every timestep and in each cells of the mesh, the dust temperature that is obtained solving Eq. (8) is compared with the local evaporation temperature of the dust grains T_{evap} . It is initially determined in Pollack et al. (1994) and has been reformulated in Isella & Natta (2005) as the power-law expression $T_{\text{evap}} = g\rho^\beta$ where $g = 2000 \text{ K}$ and $\beta = 0.0195$. It permits to adjust the local dust-to-gas mass ratio by taken into account the evaporation ($T > T_{\text{evap}}$) and the sublimation ($T < T_{\text{evap}}$) of the dust grains component of our mixture treated as a single-fluid. It particularly applies to the hot regions of the computational domain such as in the innermost part of the disc, see Kuiper et al. (2010).

The stellar luminosity represents the total irradiation, i.e. the sum of the photospheric luminosity L_\star plus the accretion luminosity $L_{\text{acc}} \propto \dot{M}_\star \dot{M}/R_\star$ of the central protostar. This quantity is mainly a function of the stellar radius R_\star , the effective temperature T_{eff} and the accretion rate \dot{M} that are interpolated from the pre-main-sequence stellar evolutionary models assuming high accretion of Hosokawa & Omukai (2009). The tracks allow us to time-dependently adapt the protostellar luminosity as a function of the accretion history onto the forming massive star.

The gravity of the gas is taken into account calculating the total gravitational potential felt by a volume element of the gas,

$$\Phi_{\text{tot}} = \Phi_\star + \Phi_{\text{sg}}, \quad (9)$$

where $\Phi_\star = -GM_\star/r$, with M_\star the protostellar mass and G the universal gravity constant. The self-gravity of the gas Φ_{sg} is described by the Poisson equation,

$$\Delta \Phi_{\text{sg}} = 4\pi G\rho, \quad (10)$$

that we solve separately. This allows the simulation to tend towards a solution which reports both the accretion phenomenons onto the central protostar but also the gravitational interactions that disc substructures share with each other. No additional artificial shear viscosity is injected into the system, via e.g. an α -prescription of Shakura & Sunyaev (1973), since three-dimensional models produce self-consistently gravitational torques accounting for efficient angular momentum transport (Kuiper et al. 2011; Hosokawa et al. 2016).

2.2 Grid, boundary conditions and numerical scheme

We perform our three-dimensional numerical simulations using a static, non-uniform grid mapped onto a spherical coordinate sys-

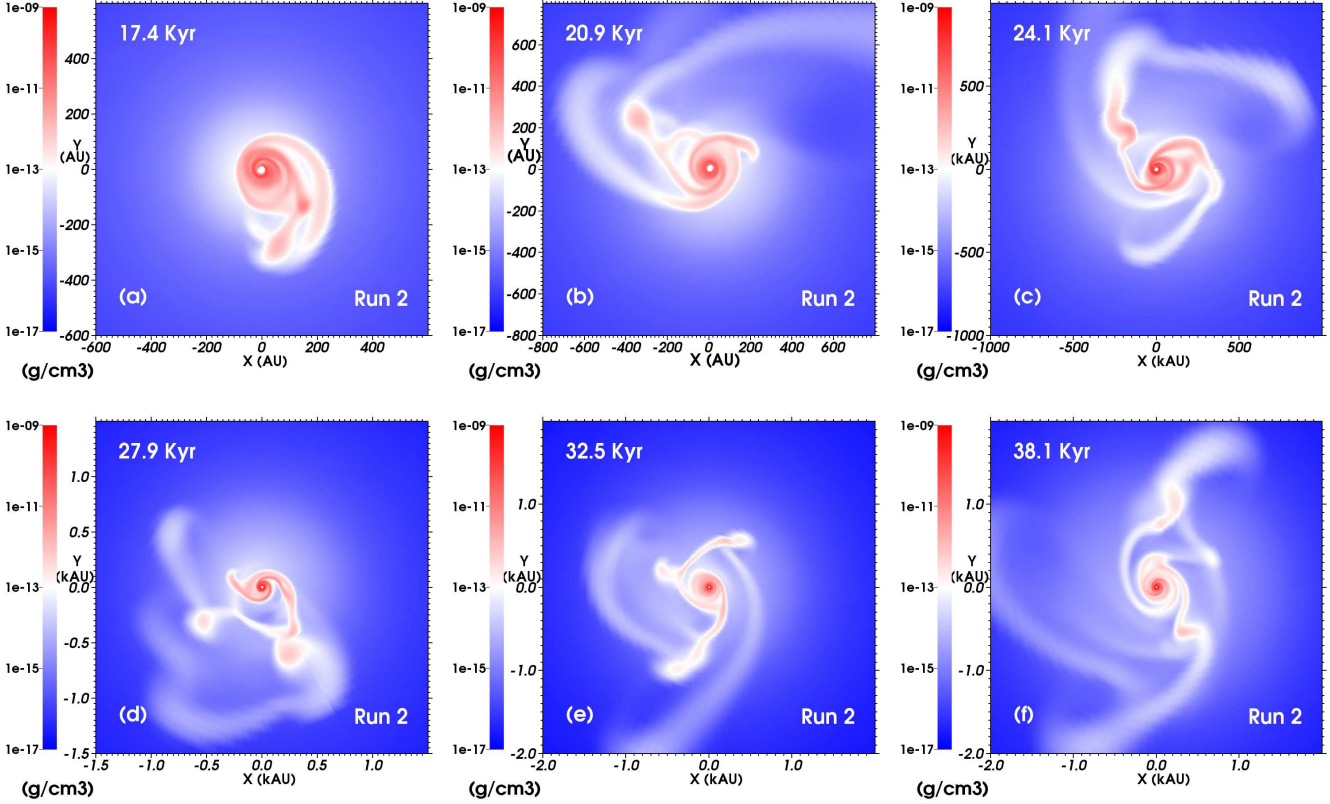


Figure 2. Similar to Fig. 1 for Run 2.

tem (r, θ, ϕ) . Assuming mid-plane symmetry of the computational domain with respect to $\theta = \pi/2$, the grid size is $[r_{\text{in}}, r_{\text{max}}] \times [0, \pi/2] \times [0, 2\pi]$ along the radial, polar and azimuthal directions, respectively. The grid is made of $128 \times 21 \times 128$ cells so that we use squared cells in inner region of the midplane. The mesh is logarithmically stretched in the radial direction, i.e. their size radially increases as $r(10^f - 1)$ with $f = \log(r_{\text{max}}/r_{\text{in}})$, and it expands as $\cos(\theta)$ in the polar direction (Ormel et al. 2015) whereas it is uniform along the azimuthal direction. This grid choice allows us to save computing time in reducing the total number of cells while having both a high spatial resolution of up to $\Delta r < 1\text{AU}$ in the inner region of the midplane. Particularly, the grid resolution is at below 10 AU in the $\approx 500\text{AU}$ region of the domain. The inner boundary in $r_{\text{in}} = 10\text{AU}$ whereas the outer one is $R_c = 0.1\text{pc}$. Outflow conditions are assigned at both boundaries of the radial directions so that we can on-the-fly estimate, e.g. \dot{M} as the mass of the material crossing r_{in} .

We solve the above described equations using the PLUTO code (Mignone et al. 2007, 2012) that has been augmented with several modules for self-gravity, radiation transport and stellar evolution that are described in Kuiper et al. (2010, 2011); Kuiper & Yorke (2013b). The distinctive feature of this method consists in carefully treating the stellar radiation, first ray-tracing the photons from the stellar atmosphere to the disc and then mimicking their propagation into the disc by flux-limited diffusion (see also Kuiper et al. 2012; Kuiper & Klessen 2013). This algorithm has shown the existence of a dust-free front in the massive stars' surroundings (Kuiper et al. 2010) and this has been strengthened by semi-analytical calculations (Vaidya et al. 2011).

Our method uses a Godunov-type solver made of a shock-

capturing Riemann solver embedded in a conservative finite-volume scheme. We use the hllc solver for fluid dynamics that is ruled by the Courant-Friedrich-Levy parameter set to $C_{\text{cfl}} = 0.1$ (Run 3, see Section 3) and to higher initial values ($C_{\text{cfl}} = 0.2-0.3$) for the other runs. Furthermore, we use the minmod flux limiter and the WENO3 interpolation scheme with the third order Runge-Kutta (RK3) time integrator. Additionally, we use the FARGO (Fast Advection in Rotating Gaseous Objects) method (Masset 2000) which permits larger timesteps than if exclusively controlled by a strict application of the Courant-Friedrich-Levy rule. FARGO has been designed to be utilised in the context of problems with a background orbital motion like our simulations and it is available in PLUTO (Mignone et al. 2012). Therefore, our overall scheme is third order in space and time. To reduce the huge computing time of such calculations, the radiation transport is performed within the gray approximation. The self-gravity of the gas is calculated up to reaching $\Delta\Phi_{\text{sg}}/\Phi_{\text{sg}} \leq 10^{-5}$ as in Kuiper et al. (2011). Finally, note that the seed perturbations for the non-axisymmetric modes are numerical (cf. Kuiper et al. 2011; Hosokawa et al. 2016).

3 INITIAL CONDITIONS

In this section, we present the initial internal structure of the pre-stellar core of our numerical calculations. We first describe the gas density and velocity distribution laws that we consider, before presenting our models and their respective initial characteristics.

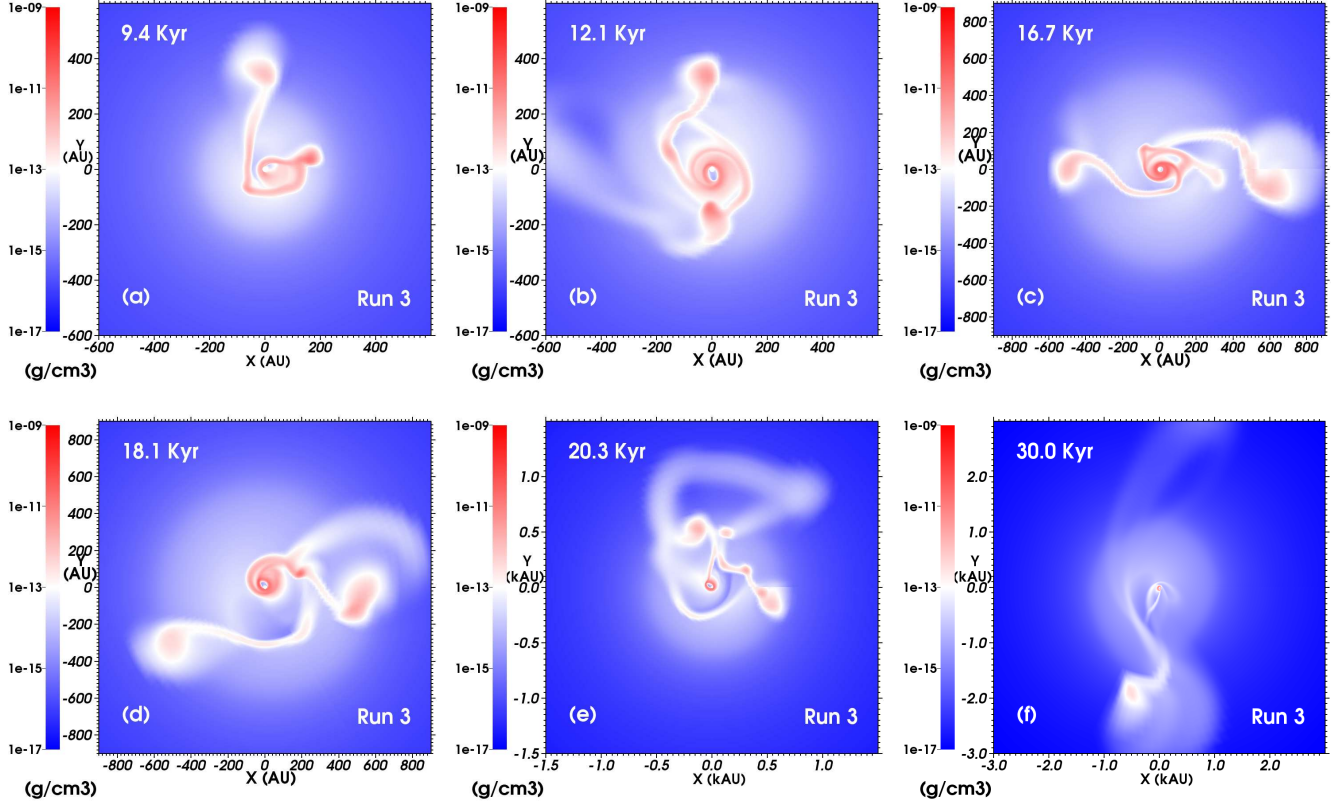


Figure 3. Similar to Fig. 1 for Run 3.

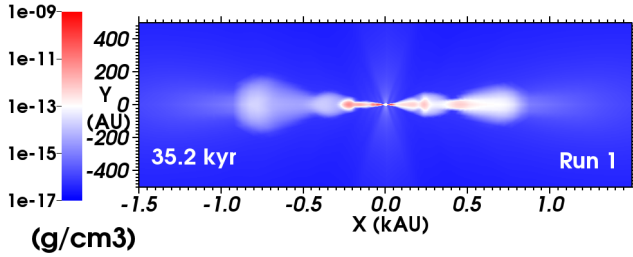


Figure 4. Vertical density structure (in g cm^{-3}) of the accretion disc generated in Run 1 at a time 35.2 kyr and shown with $\phi = 0$. The density is plotted on a logarithmic scale and the size of the figure is in (k)AU.

3.1 Gas density distribution

We consider a rotating pre-stellar core that has a radial mass density distribution $\rho(r)$ represented by the following standard power-law,

$$\rho(r) = K_\rho r^{\beta_\rho}, \quad (11)$$

where K_ρ is a function of the core size and mass and where β_ρ is a negative exponent characterizing the steepness of the density profile, respectively. The total mass of the pre-stellar core that is included between the origin of the computational domain and its outermost boundary r_{max} is $M_c = M(r = r_{\text{max}})$ where,

$$M(r) = M_c \left(\frac{r}{R_c} \right)^{\beta_\rho + 3}, \quad (12)$$

and one can therefore determine the constant K_ρ . The density distribution of the pre-stellar core is,

$$\rho(r) = \frac{(\beta_\rho + 3)}{4\pi} \frac{M_c}{R_c^{\beta_\rho + 3}} r^{\beta_\rho}, \quad (13)$$

with r the distance to the central protostar.

3.2 Gas velocity distribution

Similarly, an angular momentum distribution is initially imposed in the pre-stellar core via a particular choice in the initial velocity field in the ϕ direction. The angular velocity profile is given by,

$$\Omega(R) = \Omega_0 \left(\frac{R}{r_0} \right)^{\beta_\Omega}, \quad (14)$$

where $R = r \sin(\theta)$ is the cylindrical radius and where β_Ω is an exponent that describes the profile such that $\beta_\Omega = 0$ corresponds to a core in solid-body rotation. The parameter Ω_0 normalizes the distribution and depends on the ratio of kinetic energy with respect to the gravitational energy $\beta = E_{\text{rot}}/E_{\text{grav}}$ that initially characterizes the system. Considering both density and momentum profiles in Eqs. (11) and (14), the gravitational energy of the pre-stellar cloud is,

$$E_{\text{grav}} = \frac{\beta_\rho + 3}{2\beta_\rho + 5} \frac{GM_c^2}{R_c}, \quad (15)$$

whereas its rotational kinetic energy is,

$$E_{\text{rot}} = \frac{(\beta_\rho + 3)}{(\beta_\rho + 2\beta_\Omega + 5)} \frac{\Omega_0^2 M_c R_c^{2(\beta_\Omega + 1)}}{4r_0^{2\beta_\Omega}} \int_0^\pi d\theta \sin(\theta)^{3+2\beta_\Omega}, \quad (16)$$

which must be integrated numerically. Finally, one can, for a given molecular cloud characterized by a choice of M_c , β_ρ and β_Ω and fixing the desired ratio β , find the corresponding Ω_0 .

3.3 Models presentation

The momentum distribution is initially implemented into the code via the ϕ component of the velocity $v_\phi(R) = R\Omega(R)$ while the other components of the velocity field are $v_r = v_\theta = 0$. We assume that the percentage of kinetic energy with respect to the gravitational energy is $\beta = 4\%$ for all three models. Additionally, we assume that the dust is coupled to the gas with a gas-to-dust mass ratio of 100. The thermal pressure is set to $p = R\rho T_c/\mu$ with R the ideal gas constant, μ the mean molecular weight and $T_c = 10$ K the temperature of the pre-stellar core. The dust temperature T_d is considered as equal to the gas temperature $T_g = T_d = T_c$. We run three simulations (our Table 1) initially setting the density distribution $\beta_\rho = -3/2$ that is a typical value for a collapsing pre-stellar core that generates a present-day massive protostar (van der Tak et al. 2000; Mueller et al. 2002). The difference between simulations concern the initial angular velocity distribution of the pre-stellar cloud, which is $\beta_\Omega = 0$ (Run 1, cf. Klassen et al. 2016), $\beta_\Omega = -0.35$ (Run 2) and $\beta_\Omega = -3/4$ (Run 3). Run 3 is the same simulation as in Meyer et al. (2017), but with a longer run-time. Our simulations explore the parameter space in terms of initial angular frequency distribution $\Omega(R)$ at fixed M_c , R_c , T_c , β and β_ρ . Additionally, we perform three other models with the same initial conditions as Run 1, but without protostellar irradiation (Run 1-noIrr), with a lower spatial resolution using a grid of $64 \times 11 \times 64$ cells (Run 1-LR) and with a higher spatial resolution using a grid of $256 \times 41 \times 256$ cells (Run 1-HR) (see Section 5).

4 ACCRETION DISC FRAGMENTATION

In this section, we analyze the properties of the collapsing pre-stellar cores. We follow the evolution of the density fields in the simulations and discuss their differences before describing the fragmentation of the accretion discs. For each model, we look at the accretion rate onto the protostar and its feedback to the disc as accretion-driven outbursts.

4.1 Accretion disc fragmentation and protostar evolution

In Figs. 1, 2 and 3, we plot the midplane density field (in g cm^{-3}) from our models Run 1, 2 and 3 at six different representative evolutionary times (in kyr) elapsed since the beginning of the simulations. The figures show the inner region of \approx few (k)AU around the protostar, while the computational domain is much more extended ($R_c = 0.1\text{pc}$). Every figure corresponds to times after the formation of the disc at times 11.5, 7.2 and 3.7 kyr for our models Run 1, Run 2 and Run 3, respectively, once pre-stellar core material orbits the protostar with approximately Keplerian velocity. Despite of the fact that the overall evolution of the discs is globally similar, sensitive morphological differences appear. The accretion discs develop spiral arms under the effects of gravitational instability and

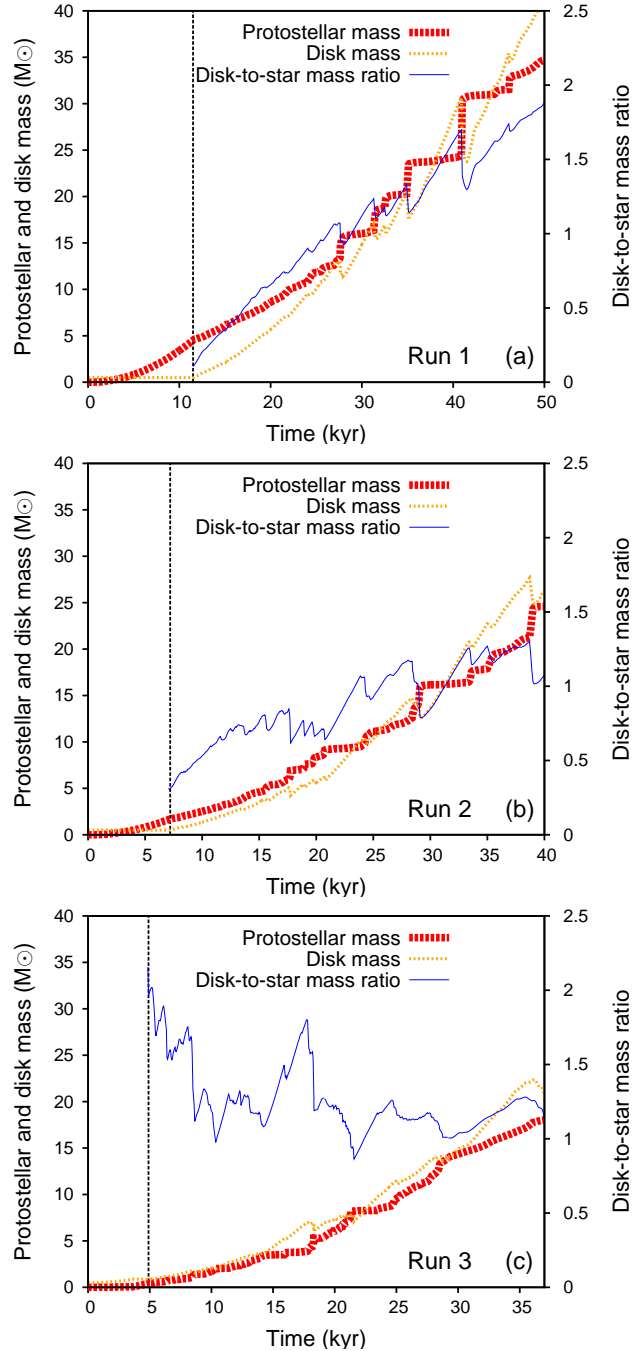


Figure 5. Protostellar mass, disc mass and disc-to-star mass ratio evolving with time. Vertical lines mark the end of the free-fall collapse and the onset of the disc formation.

the discs adopt the typical filamentary structure of self-gravitating systems under the effects of rotation (Lodato 2007).

The discs are rather compact if $\beta_\Omega = 0$ (Run 1) and more extended if the initial angular velocity distribution is steeper, because it favours the fast growth of large spiral arms, e.g. if $\beta_\Omega = -0.75$ (Run 3). All discs strongly fragment by developing inhomogeneous regions in their spiral arms, however, discrepancies arise with the distribution of those circumstellar clumps, as seen in Figs. 1-3. While orbiting the protostar in their host spiral arm, the clumps can migrate to larger radii or rapidly move inwards under the effects of

gravitational torques, before disappearing into the sink cell. Note that the overdensity at ≈ 200 AU from the sink cell in the spiral arm of Fig. 3d is subject to a rapid migration onto protostar that is described in detail in Meyer et al. (2017). This scenario of falling clumps repeats itself throughout the integration time of all models. Particularly, this mechanism is responsible for the variable accretion onto the protostar and it governs its mass evolution (see section 7.1).

Fig. 5 plots time evolution of the mass of the protostars (in M_\odot , thick dotted red line). We measure the mass of the discs (in M_\odot , thin dotted yellow line) and the disc-to-star mass ratio (thin solid blue line) in our simulations Run 1 (a), Run 2 (b), and Run 3 (c) by considering the material in a cylinder of radius 1500 AU and height 500 AU centered at the origin and perpendicular to the disc, as suggested by Klassen et al. (2016). Such a cylinder contains the discs throughout their evolution (see Fig. 4). The vertical dotted black line marks the time of the onset of the disc formation. The mass of our protostars monotonically increases as a function of time with a slope corresponding to accretion rate of circumstellar material. The periods of smooth mass increase, e.g. at times between 11.5 kyr and 26.5 kyr (Fig. 5a) is produced by the baseline (but variable) accretion rate generated when non-fragmenting portions of spiral arms wrap and vanish into the sink cell (Fig. 1a). This dominates the mass accretion at the time of disc formation and during the early disc fragmentation. At later times, the stellar mass evolution experiences sudden increases of up to a few solar masses, e.g. at times 27.6, 35.1 or 41.0 kyr, which marks the accretion of clumps.

As our model with solid-body rotation forms a disc that is smaller in size, it produces more fragments, which in turn generate a larger number of step-like jumps in the protostellar mass history (Fig. 5a) than the other runs (Fig. 5b,c). The computational cost of our simulations increases as a function of the steepness in the initial velocity distribution, which is the only parameter differentiating Runs 1–3. Consequently, we can have long integration times for the model with solid-body rotation and form a $35 M_\odot$ protostar while the other stars reach only 25 and $18 M_\odot$, respectively. The disc mass evolves accordingly, with sudden decreases when a clump leaves the disc to fall onto the protostar (see Section 4.2). The disc-to-star mass evolution reports the simultaneous increases of the protostellar and disc mass. Importantly, the disc fragmentation does not prevent accretion onto the protostar.

4.2 Variable accretion onto the protostar

Fig. 6 displays the accretion properties of the systems. The figure shows the accretion rate (in $M_\odot \text{ yr}^{-1}$, from the envelope onto the disc measured at $r = 3000$ AU (cf. Meyer et al. 2017), thick dotted red line) and the accretion rate onto the protostar (in $M_\odot \text{ yr}^{-1}$, thin solid blue line) in our Run 1 (a), Run 2 (b), and Run 3 (c). As a result of disc formation and its subsequent fragmentation, mass accretion onto the protostar is highly variable. The variety of lengths and sizes of the filaments and gaseous clumps accreted by the protostar generates the variability of \dot{M} . This has already been found in several previous numerical studies, e.g. devoted to low-mass star formation (Vorobyov & Basu 2007; Machida et al. 2011; Vorobyov & Basu 2015), and in the context of primordial star formation (Vorobyov et al. 2013). When a dense circumstellar clump falls onto the protostar, violent accretion spikes happen thanks to the mechanism depicted in Meyer et al. (2017). All models have such remarkable accretion peaks, with increases of the accretion rate up to about a few $10^{-1} M_\odot \text{ yr}^{-1}$ over a time interval

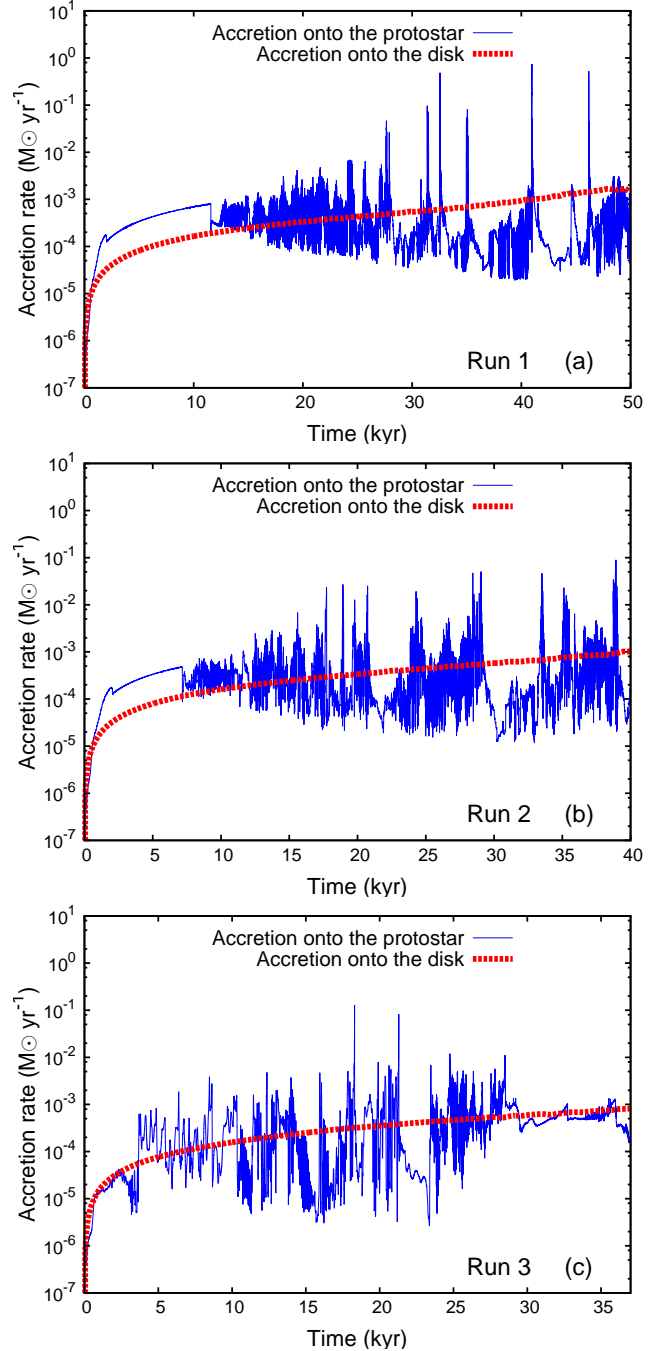


Figure 6. Accretion rates onto the protostar-disc systems.

of ≈ 20 yr. The time interval separating the accretion spikes corresponds to a temporary damping of the oscillations of the accretion rate induced by the leftover of the clumps which are gravitationally swung away (Meyer et al. 2017). The frequency of the occurrence of accretion bursts is about $M_{\text{cl}}/\dot{M}_{\text{d}} \approx 2\text{--}0.5$ kyr with $M_{\text{cl}} \approx 0.5\text{--} \text{few } M_\odot$ the typical mass of a circumstellar clumps and \dot{M}_{d} being the mass infall rate onto the disc.

4.3 Protostellar luminosity and accretion-driven outbursts

Fig. 7 shows the evolution of the photospheric luminosity L_\star (dotted red line) and the total luminosity $L_{\text{tot}} = L_\star + L_{\text{acc}}$ (solid blue

line) where $L_{\text{acc}} = GM_*\dot{M}/2R_*$ is the accretion luminosity of the protostar (in L_\odot) throughout our simulations Run 1 (a), Run 2 (b), and Run 3 (c). To each strong increase of the accretion rate corresponds a rise of the bolometric luminosity of the protostar, that is clearly above the mean stellar luminosity. The intensity of those accretion-driven outbursts is also influenced by the protostellar radius, i.e. a bloated protostar decreases the intensity of accretion-driven outburst since $L_{\text{acc}} \propto 1/R_*$ (Hosokawa & Omukai 2009). This explains why the relative intensity of the flares (governed by the accretion luminosity at times ≥ 25 –30 kyr) does not correspond to the relative strength of the associated accretion peaks, see, e.g. the forest of peaks in Figs. 6a and 7a at times ≥ 30 kyr, respectively. The bloating of the young star has not finished, i.e. much longer integration times of the system, ideally up to the zero-age main-sequence time, is necessary in order to produce detailed statistics of accretion-driven outbursts as a function of the initial conditions of our models.

Interestingly, Run 3 does not have further accretion peaks after times ≥ 28 kyr, at least for the integration times that we consider. This model generates our more extended disc of radius ≈ 4 kAU, which develops structures resembling a second accretion disc bridged by a gaseous filament. By second disc we mean that the circumstellar clump concerned, while rotating, migrates to radii larger than ≈ 2 kAU and begins accreting from the primary disc but also from the still collapsing pre-stellar core material, such that the clump forms its own accretion disc (not properly resolved by our logarithmic grid at this distance from the primary protostar), see also simulations of Offner et al. (2010); Kratter et al. (2010). The midplane density field suggests that it may be due to the formation of a massive binary star of separation ≈ 2 kAU (Fig. 3f), however, our logarithmically-expanding grid in the radial direction does not resolve the Jeans lengths at such large radii from the central protostar and, consequently, it does not allow us to conclude on this with more certitude. Our series of models show that the phenomenon of accretion-driven outbursts is a general feature of the parameter space in terms of initial angular velocity distribution. It stresses the very close similarities existing between the variability of forming massive stars and the other regimes of star formation, see the extended literature about the formation of low-mass stars (Vorobyov & Basu 2010, 2015) and primordial stars (Stacy et al. 2010; Greif et al. 2011, 2012; Hosokawa et al. 2016; Sakurai et al. 2016). Further work will provide us with more statistics on luminous accretion-driven outbursts to be compared with the FU-Orionis-like outburst of S255IR (Burns et al. 2016; Caratti o Garatti et al. 2016).

5 PHYSICAL AND NUMERICAL EFFECTS

The role of the incident protostellar radiation and effects of the spatial resolution on the fragmentation of an accretion disc formed around a young high-mass star are examined in this section.

5.1 Effects of protostellar irradiation

Fig. 8 compares the accretion rate history (a) and the protostellar mass evolution (b) of two models with $\beta_\Omega = 0$. Run 1 considers the protostellar radiation feedback in addition to the radiation transport in the accretion disc (thin blue solid line) while Run 1-noIrr ignores the protostellar irradiation (thick dotted red line). The mean accretion rate onto the central growing star is similar in both cases,

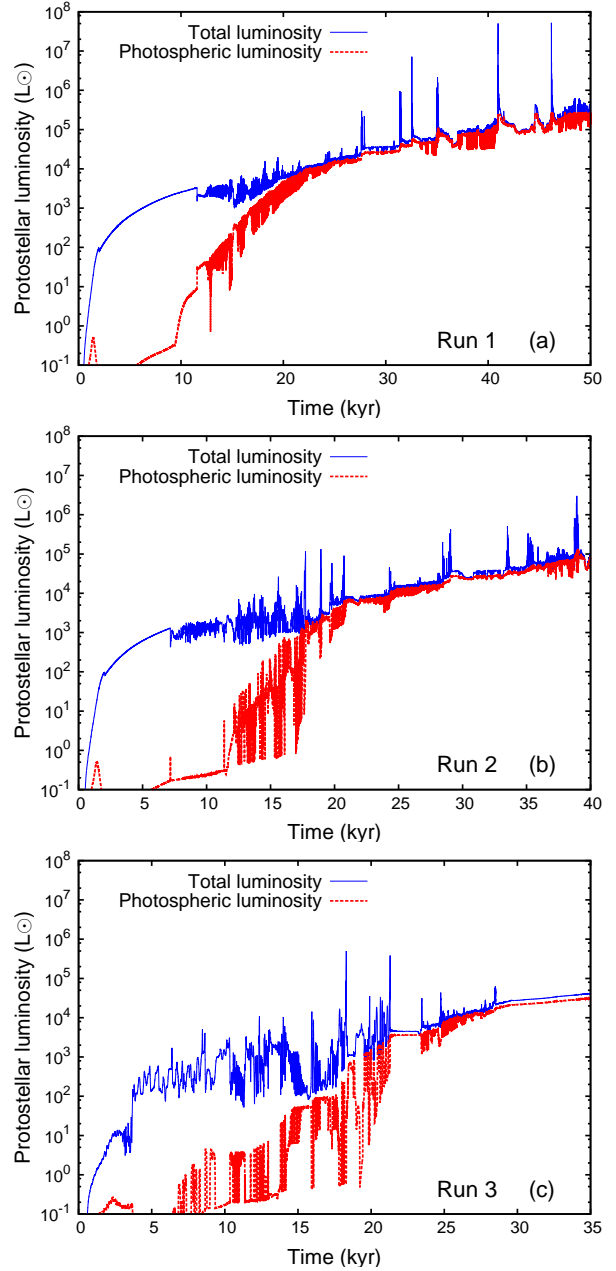


Figure 7. Bolometric protostellar luminosities (blue solid lines) and photospheric emission of our protostars (dotted red lines). The lightcurves report the changes in the accretion rates of Fig. 6.

with a mean value of about $10^{-4} - 10^{-3} M_\odot \text{ yr}^{-1}$ and lowest values of $\approx 5 \times 10^{-5} - 5 \times 10^{-4} M_\odot \text{ yr}^{-1}$. The absence/presence of stellar feedback does not prevent regular accretion spikes in the mass accretion rate from developing (Fig. 8a). In the non-irradiated case, the accretion bursts are more numerous, appear sooner and are of higher mean intensity than their irradiated counterparts, although no remarkable spikes reaching intensities of more than a few $10^{-1} M_\odot \text{ yr}^{-1}$ happen, as in Run 1.

This indicates an earlier but more violent fragmentation of the disc of Run 1-noIrr as compared to the irradiated disc of Run 1. Once fragmentation is triggered (at times larger than 30 kyr), the variable accretion rate reaches values slightly higher than in the non-irradiated case. However, once the first accretion-driven out-

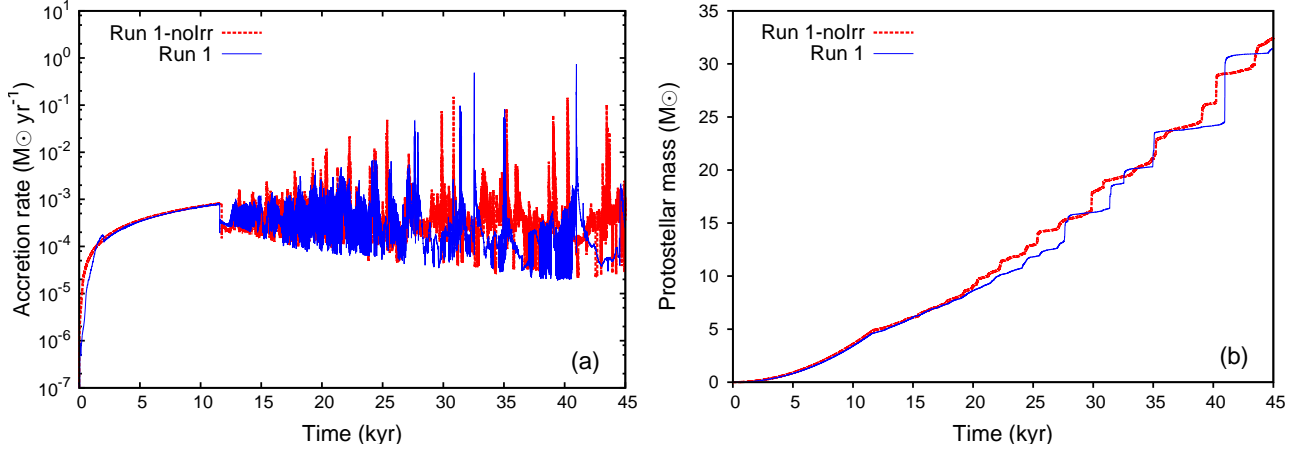


Figure 8. Comparison between the accretion rate (a) and the mass evolution (b) of a model considered with (Run 1) and without irradiation (Run 1-noIrr).

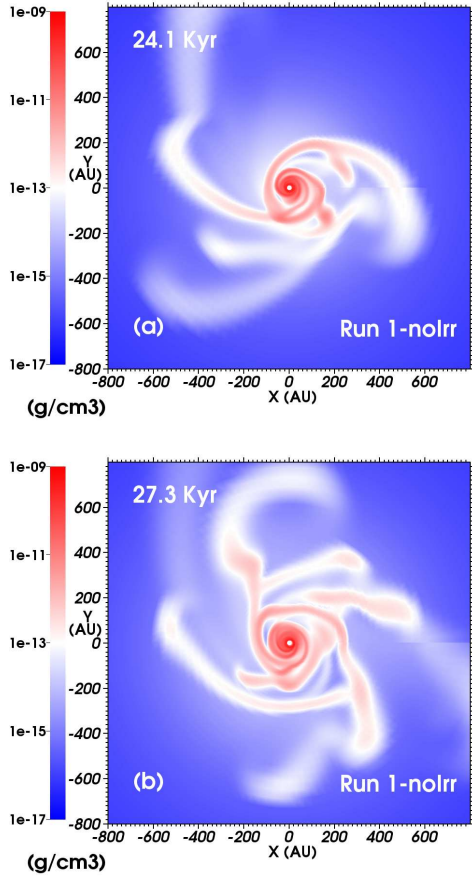


Figure 9. Midplane density field of the model with initial solid-body rotation ($\beta_{\Omega} = 0$) modelled without protostellar irradiation (Run 1-noIrr).

bursts take place, both stellar mass histories are very analogous for times ≤ 18 kyr (Fig. 8b), with differences arising later. Indeed, despite of this similar qualitative stellar mass evolution ending with the formation of a star of mass $> 30 M_{\odot}$ at times ≥ 45 kyr, Run 1-noIrr globally reports a higher number of step-like increases of M_{\star} . They correspond to the accretion of a larger number of dense circumstellar clumps. One can notice that the migrating gaseous

clumps are of smaller individual mass in Run 1-noIrr, leading to less intense accretion spikes compare to those of Run 1 (Fig. 8a). This is consistent with the disc being of lower temperature, having smaller Jeans length and thus lower-mass clumps.

Fig. 9 shows two snapshots of the midplane density field of Run 1-noIrr, at times 24.1 and 27.3 kyr. The figures correspond to times before (a) and after (b) the initial fragmentation of the disc in Run 1 (Figs. 1a,b). This time interval brackets the formation of the first fragment in the simulation of the accretion disc with irradiation (Run 1). When stellar feedback is considered, the disc is still stable at time a 24.1 kyr (Fig. 1a) while in the case without incident protostellar radiation it has already multiple distinct spiral arms (Fig. 9a) in which develop overdense regions (Fig. 9b) that are responsible for the formation of (migrating) circumstellar clumps, producing the accretion-driven bursts in Fig. 8b. Earlier disc fragmentation happens since the close surroundings of the non-irradiated disc are colder and therefore fragment faster. Our comparison models illustrate the role of the direct protostellar heating in the stabilization of self-gravitating accretion discs around young high-mass stars.

5.2 Effect of resolution

Fig. 10 plots the midplane density field in Run 1-LR (left), Run 1 (middle) and Run 1-HR (right) at times 24.1 (top panels), 27.3 kyr (cf. Run 1 in Fig. 1a,b), and at times > 30 kyr (bottom panels), when the fragmentation process is already triggered. In all three models, the disc at a time of 24.1 kyr has the shape of twisted spiral of distance about 350-400 AU from the protostar (Fig. 10a-c). The innermost part of the disc is more resolved in Run 1 than in Run 1-LR and has numerous thin arms spiraling around the sink cell (Fig. 10b), while Run 1-HR has just exhibited the first formation signs of denser substructure in its outer arm (Fig. 10c). At time 27.3 kyr one can see that extended spiral arms have already grown. The lowest resolution model (Run 1-LR) does not show traces of undergoing substructure formation (Fig. 10d) while Run 1 has portions of spirals arms including the curved, denser sections (Fig. 10e). Since the only difference between all models is the grid resolution, one can directly estimate the effect the spatial resolution has on disc fragmentation. The highest resolution model evolves similarly, except that the first fragment forms and migrates sooner (Fig. 10f). At times > 30 kyr, the patterns show either spiral arms (Fig. 10g), or fragments in the case of the most-resolved model (Fig. 10i). The bottom line of panels illustrates the effects of

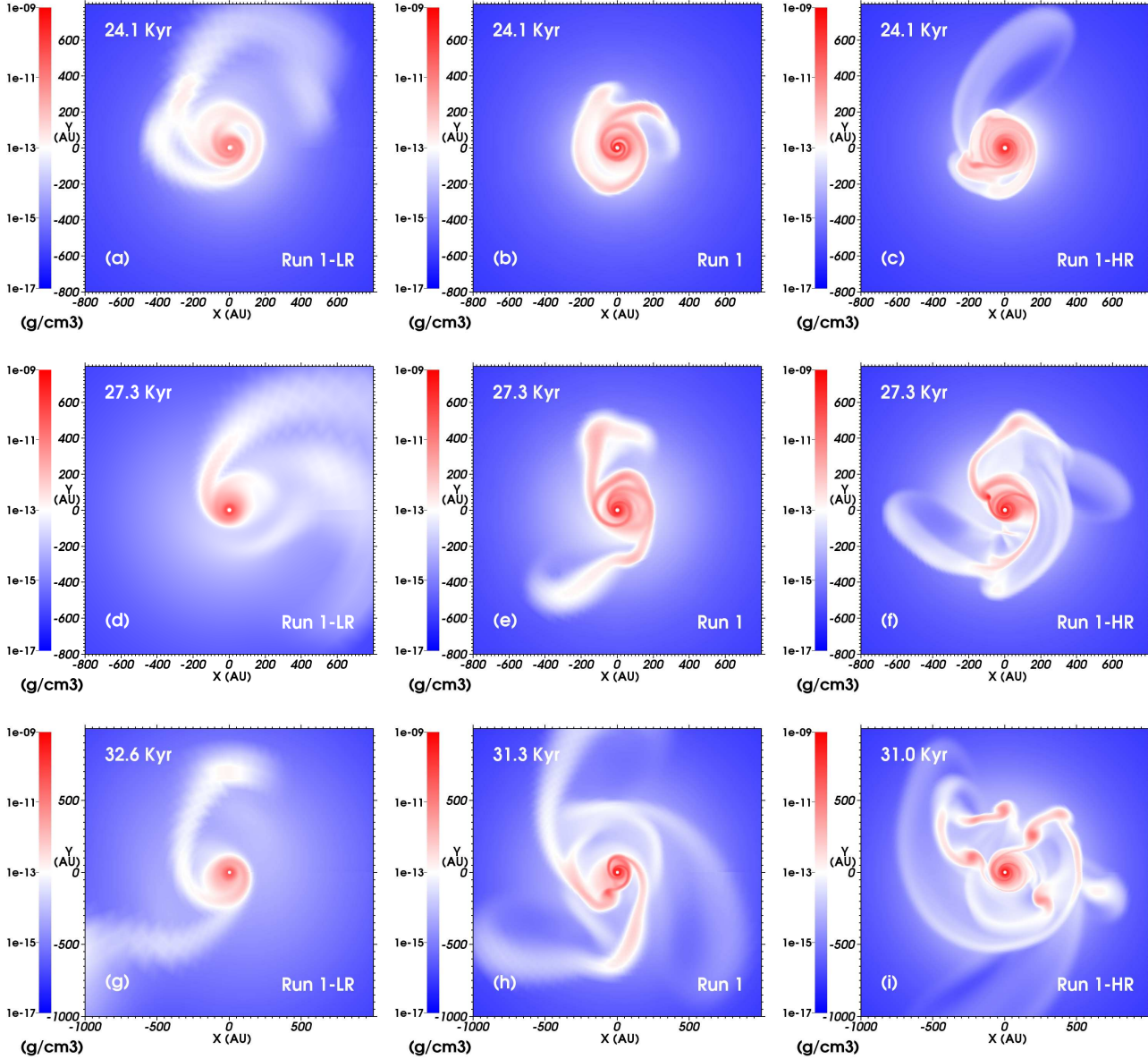


Figure 10. Density fields of models with initial solid-body rotation, considered with different spatial resolution (Run 1-LR, Run 1 and Run 1-HR).

spatial resolution on the random development of the disc structures once the fragmentation process begins. Using the finest grid resolution to date, we point the prime importance for the treatment of the close stellar environment for reliability of numerical disc fragmentation studies. This was expected from comparison with disc fragmentation studies in the low-mass star formation regime where the irradiation is negligible, see e.g. Lichtenberg & Schleicher (2015), but also from models in the context of primordial star formation, in which stellar feedback is efficiently at work, see Greif et al. (2011); Vorobyov et al. (2013); Machida & Nakamura (2015) and the Fig. 3 of Hosokawa et al. (2016) for a resolution study.

Fig. 11 is similar to Fig. 8 for models Run 1 and Run 1-HR, which are our two most resolved models having an initial rigidly-rotating pre-stellar core ($\beta_{\Omega} = 0$). One can notice the good agreement between their accretion rate histories (Fig. 11a). Especially, the first remarkable accretion spike happens similarly at the times of ≈ 22 kyr showing that the solution has converged up to the for-

mation, fall and accretion of the first gaseous clumps. Further discs evolution logically differs in the sense that a higher resolution reveals the typical stochastic and fractal behaviour of fragmenting disc. The number of accretion-driven events slightly increases with the disc resolution because more clumps are formed, i.e. Run 1-HR has 3 separated spikes reaching $\geq 10^{-2} M_{\odot} \text{ yr}^{-1}$, while Run 1 has only a twin one of the same intensity (Fig. 11c). The accreted mass per unit time is similar in both models and the mass evolution of the central protostar converges up to ≈ 22 kyr, the time of the first clump migration. At times < 30 kyr, the mean mass of a gaseous clump is smaller in Run 1-HR because more numerous but lighter fragments form in the disc, and large accretion events are replaced by the successive accretion of lighter fragments for a roughly equal total mass, see for example at times ≈ 26 -29 kyr (Fig. 11b).

We have performed a resolution study by increasing the resolution of our models up to the highest spatial resolution to date. The above presented elements show that our solutions are sufficient to

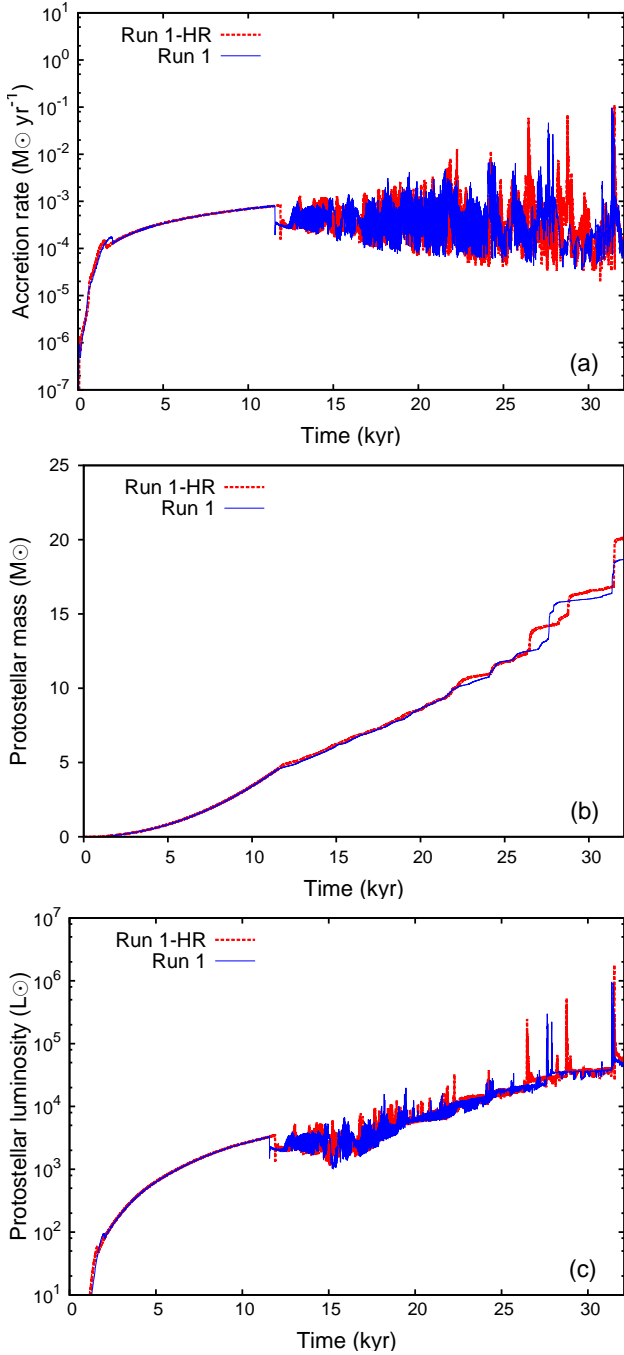


Figure 11. Comparison between the accretion rate (a) and the mass evolution (b) and the luminosity (c) of a model with several grid resolutions.

extract the parameters required for our analyses and conclusions in terms of accretion variability, inner disk fragmentation and migrating gaseous clumps.

5.3 Jeans length resolution

This paragraph investigates our discs with respect of the Truelove criterion (Truelove et al. 1998), which stipulates that the local Jeans length must be resolved by at least 4 grid cells. The so-called Jeans

number is defined by,

$$n_J = \frac{\Delta}{\lambda_J}, \quad (17)$$

where,

$$\lambda_J = \left(\frac{\pi c_s^2}{G\rho} \right)^{1/2}, \quad (18)$$

is the Jeans length and Δ is the grid cell size. Therefore the Truelove criterion reads,

$$\frac{1}{n_J} = \frac{\lambda_J}{\Delta} \geq 4, \quad (19)$$

and the clump-forming regions of the disc must satisfy this relation. Fig. 12a-c shows the minimal disc midplane inverse Jeans number $1/n_J$, estimated from different simulation snapshots and plotted as a function of the radial direction for the inner 1000 AU which is the typical size of our discs. The hatched region in the figures indicates values $1/n_J < 4$ where the Truelove criterion is violated. Run 1 is fully resolved in the inner 1000 AU of the disc (red thick dotted line). The minimal inverse Jeans number exhibits variations corresponding to the presence of the dense spiral arms hosting circumstellar clumps (local minimum) and the underdense regions between the spiral arms (local maximum). Note that the mean value of the azimuthally averaged inverse Jeans number is much larger (thick solid orange line). High resolution simulation Run 1-HR is our best Truelove-resolved model (green thick dashed line). This criterion is a minimal requirement to consider simulations of self-gravitating discs are numerically reliable. It does not consist of a strict convergence rule, as illustrated by the density pattern differences of the Truelove-resolved models Run 1 and Run 1-HR.

Fig. 12b is similar to Fig. 12a but for Run 1, assuming different grid types and resolutions. The thick dotted red line assumes the logarithmic simulation grid while the other lines considers minimal inverse Jeans lengths calculated with our disc midplane density field together with uniform grids of resolution $\Delta = 10$ -40 AU, corresponding to the resolution typically reached by codes with Cartesian grids for this kind of simulations. The logarithmic grid is better than any considered uniform grid up to radii of about 150-200 AU, which is similar to the inner disc size after simulation times of ≈ 23 -30 kyr, depending on the models. Particularly, the resolution $\Delta = 40$ AU is not able to reach our disc resolution up to radii of ≈ 600 -800 AU. This means that substructures of the disc in Run 1 can not be reproduced with such a grid size, as the onset of clump formation and migration happens in spiral arms at a typical distance of a few hundreds AU from the central protostar (see Meyer et al. 2017). This resolution-dependence of the numerical capture of accretion-driven outbursts phenomenon explains why it could not be captured by mesh refinement codes with a Cartesian grid since their maximum disc resolution of 10 AU is so far coarser in the inner disc than in our simulations (see e.g. Krumholz et al. 2007b; Klassen et al. 2016; Rosen et al. 2016). Fig. 12c is similar to Fig. 12b but for Run 1-HR at different times of its evolution, corresponding to the snapshots in Fig. 10c,f and j. Throughout the whole simulation time, this model is well Truelove-resolved ($1/n_J \geq 10$), even when clumps start flourishing at the outskirts of the disc ($1/n_J \geq 4$ -6, see Fig. 13). The necessary resolution of the Jeans number in the clump cores is achieved partly because they evolve in the disc midplane, see Fig. 12a-c. In all our simulations, we generally find values of $\lambda_J/\Delta \sim 6$ -8, see details relative to the first migrating clump of Run 3 in Meyer et al. (2017).

The equatorial symmetry of our setup forces the clump to de-

velop and evolve within the midplane. While this prevents clumps from potentially scattering to high disc latitudes. Indeed, clumps are therefore resolved at all radii with the smallest grid cells permitted by the used cosine-like grid along the polar direction. The disc scale height in the clump-forming regions is $H \approx 10$ AU and can increase with r up to $H \approx 100$ AU in the outer disc region. The choice of an expanding grid resolution $\Delta(r)$ allows us to resolve the disc scale height $H(r) \gg \Delta(r)$ and at the same time to reduce the number of cells and the computing time of the simulations. The Hill radii of the clumps, i.e. the surrounding regions that is gravitationally influenced by their mass, is $R_H \approx 64 - 96$ AU for a clump mass of $M_{cl} \approx 1.0 M_\odot$ located at $r \approx 200 - 300$ AU from a star of $M_\star \approx 10 M_\odot$, whereas the grid resolution is of $\Delta \simeq$ a few AU at that radius in our Runs 1-3 (and a factor of 2 smaller in Run 1-HR). The Hill radius goes as $R_H \approx r(M_{cl}/3M_\star)^{1/3}$ and therefore increases at larger radii, which compensates the linear loss of resolution of the logarithmically expanding grid compared to the inner part of the disc. As the protostar grows, M_\star increases and assuming $M_\star \approx 30 M_\odot$ we find $R_H \approx 45 - 67$ AU, which is still correctly resolved. As the clump falls in, it loses mass but the grid resolution increases; leading to similar conclusions as above. What is new in the present study is not the included microphysical processes, but the high spatial resolution allowed by the method in the innermost part of the accretion disc. We resolve the stellar surroundings better than any simulation before and explore the initial perturbations of the disc together with their effects on its subsequent overall instability.

6 HOW TO CHARACTERIZE DISC INSTABILITY?

Simulations with lower spatial resolution than used in our study often made use of sink particles to generate nascent stars in the accretion disc. Forming those sink particles underlines the assumption of disc fragmentation at this location, however, different simulation codes also apply different criteria, from density thresholds (Krumholz et al. 2007b) to the onset of local isotropic gravitational collapse (Federrath et al. 2010). Our different method, without sink particles, allows us to pronounce on the reliability of analytic criteria for disc fragmentation, by computing them for our resolved discs models and directly compare if they result in disc fragmentation. Therefore, we test the protostellar discs with respect to several criteria for the fragmentation of self-gravitating discs, i.e. the so-called Toomre, Gammie and Hill criteria. Particularly, we discuss whether those criteria are consistent with our results, and if they are necessary and/or sufficient to determine the unstable character of the discs, in the spirit of the analysis carried out in Klassen et al. (2016).

6.1 Toomre criterion

The so-called Toomre parameter measures the unstable character of a self-gravitating disc by comparing the effects of the gravity (Toomre 1963) against the combined effects of the disc thermodynamics, i.e. the gas thermal pressure, together with the rotational shear induced by the Keplerian motion of the gas, providing a stabilizing force to the system. A region of a gaseous disc is Toomre-unstable (or Q -unstable) if the dimensionless quantity,

$$Q = \frac{\kappa c_s}{\pi G \Sigma} \leq Q_{\text{crit}}, \quad (20)$$

where c_s is the sound speed of the gas, Σ the column mass density of the disc and κ the local epicyclic frequency. The aforementioned

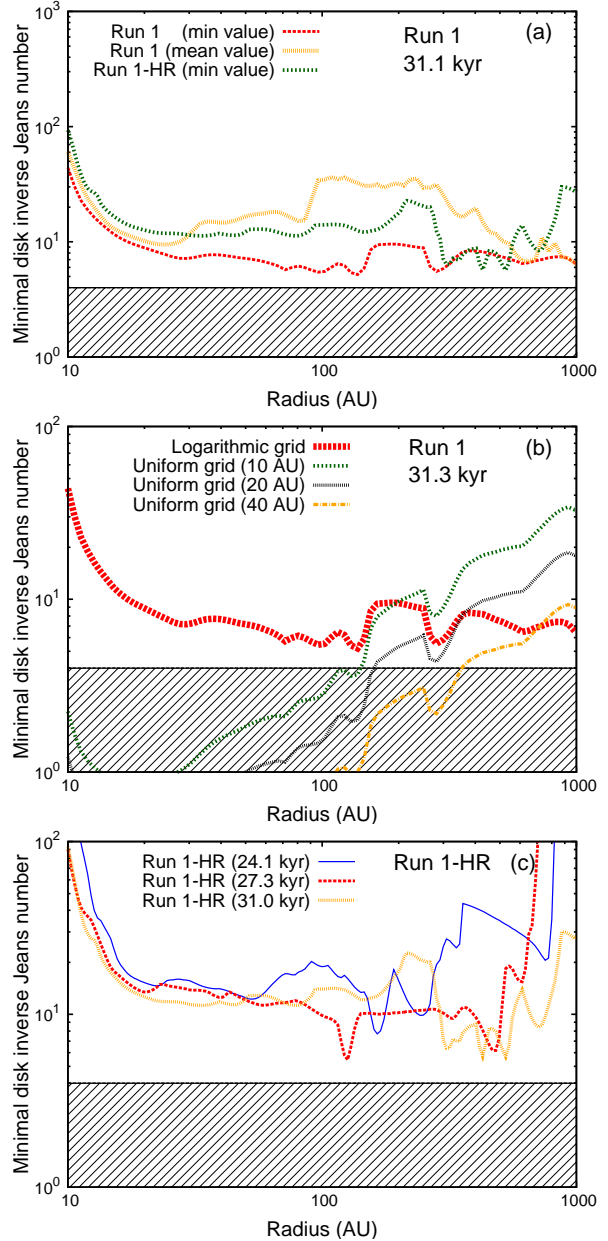


Figure 12. Minimal inverse Jeans number in the disc midplane as a function of radius. It is plotted for the resolution study involving our initially solid-body rotating simulations (a), our disc in Run 1 as considered with different grids and resolutions (b) and for our run 1-HR (c). Truelove-unresolved regions are hatched.

Toomre criterion was derived in the thin-disc limit for polytropic and axisymmetric discs, for which case $Q_{\text{crit}} = 1$. In more realistic situations, the exact value of the critical Toomre parameter Q_{crit} depends somewhat on the disc thickness, rotation curve and thermodynamics. Numerous numerical studies indicate that circumstellar discs become unstable to the growth of a spiral structure if Q becomes less than $Q_{\text{crit}} = 1.5-2.0$ (e.g. Durisen et al. 2007). When the local Q -parameter becomes smaller than 1.0, spiral arms may fragment to form compact gaseous clumps. This criterion is a necessary condition with respect to gravitational fragmentation, however, recent studies updated condition Eq. (20) to $Q < 0.6$, see the study of protoplanetary discs of Takahashi et al. (2016).

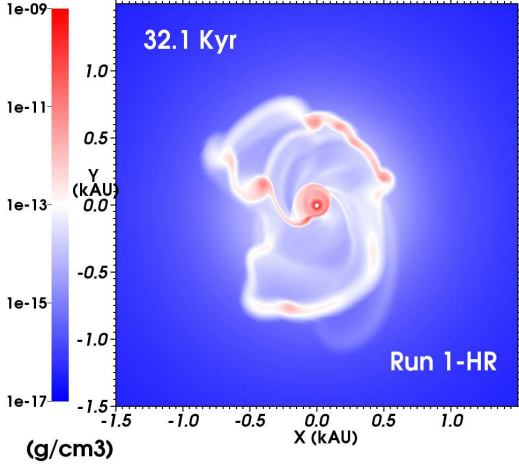


Figure 13. Midplane density field of at the end of Run 1-HR.

The middle column of panels of Fig. 14 plots the Q -analysis of the disc in our Run 1 at several characteristic timescales of its evolution. The color scale indicates whether the disc is prone to fragment ($Q \leq 1$, red), marginally unstable to fragmentation ($Q \simeq 1$, white) or stable to fragmentation ($Q > 1$, blue). Figs. 14e-h show that the Toomre criterion is satisfied by the denser regions of the spiral arms and by the circumstellar clumps in the accretion disc. The surface of the disc midplane which is prone to fragmentation increases as a function of time, as the circumstellar medium of the protostar loses axisymmetry (Figs. 14e,h). As noted in Klassen et al. (2016), the disc’s growing tendency to Q -instability comes along with an increase of the accretion variability. The ejection of the leftover of the first accreted clump, producing the first accretion-driven outburst, provokes the formation of a dense filament propagating outwards as described in fig. 1b-d of Meyer et al. (2017), which in its turn favours the generation of thin but extended spiral arms, enhancing the disc’s instability and susceptibility to experience further fragmentation events. The more violent the disc fragmentation, the lower the value of the associated local Q -parameter.

At time 24.1 kyr, the most Toomre-unstable clump located at a radius ≈ 100 AU from the protostar has $Q \approx 0.25$ –0.4 (Fig. 14d). This value is typical of the spiral arm in the discs which develop throughout our simulations. Q -values of ≈ 2.6 –3.2 in the inner region of the disc (≤ 100 AU) indicate stability, except for some very thin (but still marginally Toomre-stable with $Q \approx 1.7$) twisted spiral located at radii of ≈ 55 AU. At a time of 27.3 kyr, unstable spiral arms in the disc with $Q = 0.8$ –0.86 are noticeable, see for example the thin spiral arm at $x = -200$ AU and $y = 300$ AU in Fig. 14e. The other regions of the disc which are fragmenting into blobs have characteristics such that $Q = 0.8$ –1.2. The snapshot in Fig. 14f draws similar conclusions with multiple Q -unstable clumps of $Q \leq 0.4$ linked to each other by spiral arms which central regions can also be locally unstable ($Q \leq 0.4$ –0.5), however, most part of those arms are such that $Q = 0.8$ –1.35. Therefore, our results are consistent with the update of the Toomre criterion reported in Takahashi et al. (2016), i.e. the only necessary condition for disc instability is $Q < 0.6$, as already confirmed in the context of the stable discs shown in Klassen et al. (2016).

6.2 Gammie criterion

In the right column of panels of Fig. 14 we show maps of the so-called Gammie criterion. It locally compares the effects of the gas cooling with the hydrodynamics, i.e. the heating of the gas pressure due to the shear due to the disc rotation (Gammie 1996), and reads,

$$t_{\text{cool}}\Omega \leq \beta \approx 3 - 5, \quad (21)$$

where the local cooling timescale t_{cool} depends on the disc thermodynamics. We compute it as,

$$t_{\text{cool}} = \frac{E_{\text{int}}}{F}, \quad (22)$$

with E_{int} the internal energy in a disc column (Klassen et al. 2016) and F the radiation flux leaving the disc surface. Our protostars are surrounded by discs that are not irradiated so that they adopt the vertical isothermal structure described in Rafikov (2009), and their midplane temperature still is governed by the pressure work of the spiral arms and the radiation flux leaving the disc can be estimated as $F = \sigma T^4 / f(\tau)$ measured at the disc surface, where σ is the Stefan-Boltzman constant and $f(\tau) = \tau + 1/\tau$ is a function of the optical depth which interpolates between the optically thin ($\tau < 1$, outer part) and the optically thick ($\tau > 1$, inner part) regimes of the discs (Rafikov 2007, 2009). The figure’s color coding illustrates where the disc is β -stable ($t_{\text{cool}}\Omega \geq 3$ –5, red) or β -unstable ($t_{\text{cool}}\Omega < 3$ –5, other colours). This criterion has been numerically derived for self-gravitating discs around low-mass stars and it is subject to numerous discussions regarding the critical value of β , which has been shown to be resolution-dependent (Meru & Bate 2011, 2012) and equation-of-state-dependent (Rice et al. 2005; Clarke et al. 2007). Therefore, the existence of an universal β -value remains unclear (Lodato & Clarke 2011; Rice et al. 2012, 2014). The Gammie criterion can also be derived from the requirement that the local cooling time t_{cool} be shorter than the fastest growth time of gravitational instability $t_{\text{grav}} = 2\pi / (\Omega \sqrt{1 - Q^2})$ (Shu 1992), so that the local density enhancements can get rid of excess heat generated during gravitational contraction. In this case,

$$t_{\text{cool}}\Omega \leq \frac{2\pi}{\sqrt{1 - Q^2}}. \quad (23)$$

This form of the Gammie criterion explains the recent results of Boss (2017) arguing that disc fragmentation can take place at higher values of β given lower Q -values.

Figs. 14g-i show that our discs satisfy the Gammie criterion for instability, including the hot regions of spiral arms and gaseous clumps which are more β -stable than the interarm region, but nevertheless largely β -unstable. At the beginning of our simulations, the disc is mostly Gammie-unstable, testifying a rapid and efficient cooling of the gas, except in the very inner dense region of radius ≤ 20 –80 AU, close to the protostar, see Fig. 14g,h and Klassen et al. (2016). Throughout the simulations, the spiral arms have a typical value of $t_{\text{cool}}\Omega = 0.01$ –0.005 (Figs. 14h,i) and even lower values ($t_{\text{cool}}\Omega \ll 0.005$) in the interarm regions of the disc midplane, which means that the cooling timescale of the gas is shorter than the orbital period. Considering the both Toomre- and Gammie-unstable parts of the discs, we find that only the very innermost part of the disc does not satisfy the two criteria ($Q > 1$ and $t_{\text{cool}}\Omega \leq 3$ –5). Our results therefore agree with the analysis of the stable accretion discs around massive stars of Klassen et al. (2016) who found a low β -value in their (clumpless) discs and concluded on (i) their capacity of undergoing future fragmentation and (ii) the non-sufficiency of the Gammie criterion to distinguish fragment-

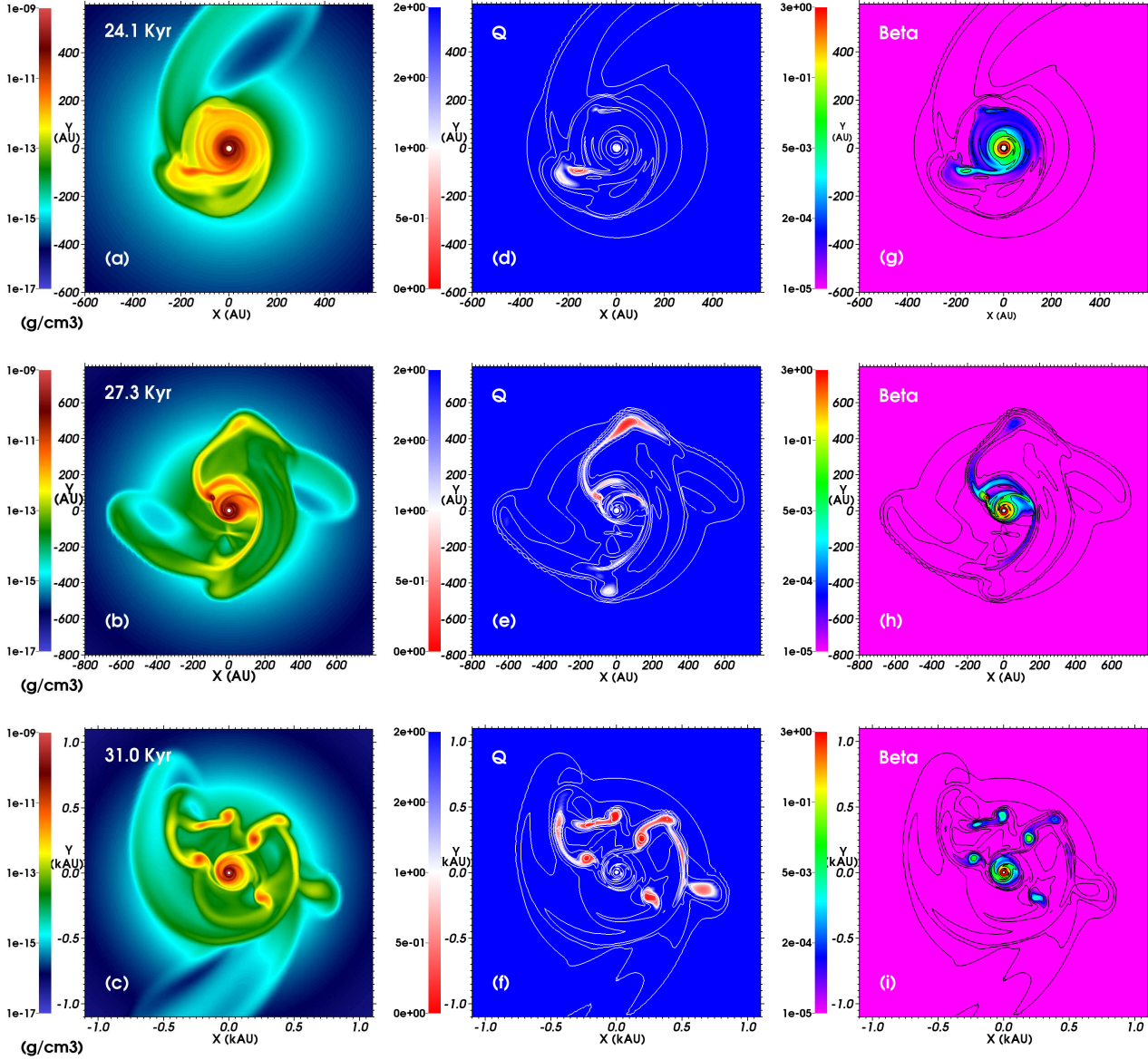


Figure 14. Density fields of Run 1-HR (left, as in Fig. 1a-c) together with corresponding Toomre Q -maps (middle) and Gammie β -maps (right).

ing from non-fragmenting regions of accretion discs around young massive stars. Note that our simulations are also in accordance with the predictions of Fig. 1 of Rafikov (2009), which concludes on the inevitable existence of a regime of disc fragmentation, located in regions at large distances from the central object in accretion discs with high accretion rates like ours, with $\dot{M} \geq 10^{-4}$ – $10^{-3} M_{\odot} \text{ yr}^{-1}$ and $\Omega \simeq 10^{-11}$ – 10^{-10} s^{-1} . Section 8.2 further discusses the usefulness of a Gammie criterion for discs around young massive stars.

6.3 Hill criterion

The so-called Hill criterion compares the effects of the self-gravity of a spiral arm with respect to the shear produced by the stellar tidal forces (Rogers & Wadsley 2012). It has been derived in the context planet embryos in protostellar discs by examining its local sphere of influence, i.e. the capacity of segment of spiral arm to further

accrete planetesimals and it has been applied with success in the context of the circumstellar medium of massive protostars (Klassen et al. 2016). A segment of a spiral arm of a given thickness l is Hill-unstable if,

$$\frac{l}{2R_{\text{Hill}}} < 1, \quad (24)$$

where,

$$R_{\text{Hill}} \approx \sqrt[3]{\frac{G\Sigma l^2}{3\Omega^2}} \quad (25)$$

is the Hill radius. The circumstellar gas that is not within twice the Hill radius of the fragment has its evolution governed by the gravity of the central protostar (Rogers & Wadsley 2012). Note that their work considered an isolated disc that was not further accreting from its pre-stellar core. This criterion turned to be more general than the Toomre and Gammie criteria because it was consistent with the apparent stability of Q - and β - unstable discs (Klassen et al. 2016).

We calculate the Hill number of a selected number of cross-sections of spiral arms in our Run 1-HR. The blobby arm of Fig. 14a gives $l = 40$ AU, $\Sigma \approx 4.19 \times 10^3 \text{ g cm}^{-2}$ and $\Omega = 3.0 \times 10^{-10} \text{ s}^{-1}$, respectively, which makes $R_{\text{Hill}} \approx 48$ AU and $l/2R_{\text{Hill}} \approx 0.41 < 1$. We repeat this analysis with the northern arm of Fig. 14b, the southern arm of Fig. 14b, the western arm of Fig. 14c and the eastern arm of Fig. 14c. With the values of $l = 29, 14, 42, 39$ AU, $\Sigma \approx 3.47 \times 10^2, 2.09 \times 10^2, 1.57 \times 10^2, 3.5 \times 10^2 \text{ g cm}^{-2}$ and $\Omega = 2.3 \times 10^{-10}, 2.7 \times 10^{-10}, 8.05 \times 10^{-11}, 5.01 \times 10^{-11} \text{ s}^{-1}$, respectively, and therefore $R_{\text{Hill}} \approx 20.1, 9.43, 54.8, 49.6$ AU and $l/2R_{\text{Hill}} \approx 0.70, 0.74, 0.38$ and $0.39 < 1$, respectively. Those numbers are in accordance with the unstable appearance of our discs and identical analysis at different times give similar results. We conclude that the Hill criterion is a reliable tool to predict the stability of self-gravitating discs around young massive stars.

7 SPECTROSCOPIC MASSIVE BINARIES FORMATION BY DISC FRAGMENTATION

Massive binaries are fundamental in the understanding of high-mass stellar evolution (Sana et al. 2012). The case of a massive proto-binary made of two young high-mass stars has been predicted (Krumholz et al. 2009a) and observed (Kraus et al. 2017). However, the formation scenario of massive binaries made of a high-mass component and a close low-mass component is so-far unexplained, although it is suspected to be closely correlated to the hierarchical multiple systems of protostars formed by disc fragmentation (Krumholz et al. 2007b; Rosen et al. 2016). This study explores such hypothesis in the context of the observed spectroscopic massive binaries (Mahy et al. 2013), a particular case of close massive binaries made of an O star with a short-period, low-mass companion which we explain by showing that disc fragmentation is a viable road for the formation of proto-O star with a short-period, low-mass companion. This section details that our simulations are consistent with the disc fragmentation channel of close/spectroscopic massive proto-binaries formation that evolve towards close/spectroscopic massive binaires once the most massive component enters the main-sequence phase of its evolution. Finally, we connect it with the phenomenon of accretion-driven outbursts in the high-mass regime of star formation.

7.1 Accretion-driven outbursts from young massive stars

Using the same numerical method as in this study, we demonstrated in Meyer et al. (2017) that disc fragmentation around young high-mass star is followed by the formation of circumstellar clumps prone to migrate and fall onto the central protostar. We previously interpreted those observable as a tracer of disc fragmentation and postulated that the recent burst from the young high-mass star S255IR-SMA1 (Caratti o Garatti et al. 2016) could be caused by the accretion of a circumstellar clump onto the protostellar surface. However, the fate of the clumps once they crossed the inner 10 AU was not calculated within our method and our conclusions are interpreted (i) by analogy with other studies on FU-Orionis(-like) outbursts from young stars and (ii) calculating the centrifugal radius of one of those circumstellar clumps. We have drawn the conclusion that accretion-driven outbursts are a general feature of massive star formation, already well-known in low-mass star formation as the FU-Orionis phenomenon (Smith et al. 2012; Vorobyov & Basu 2015) and in primordial star formation (Hosokawa et al. 2016).

This study extends the work of Meyer et al. (2017) to different

angular velocity distributions of initial collapsing pre-stellar cores. Our set of simulations includes the case of a core in solid-body rotation that has recently been associated, with the help of several fragmentation criteria, as possessing all characteristics required for disc fragmentation, despite the clear lack of fragments captured in the hydrodynamical model (see Klassen et al. 2016, and discussion on sink-particle algorithms in Section 8.3). Differences between simulations of Klassen et al. (2016) and our models mainly lies in that we avoid using sub-grid models (sink particles, see Section 8.3) and a higher spatial resolution than previously allowed by mesh-refinement codes in the close environment of the young high-mass protostar. Our models show fragmenting accretion discs whose evolution results in a pattern of clumps and filaments. This allows us to stress similarities between our results and simulations devoted to low-mass and primordial star formation. The remaining open questions consist in knowing more in detail the number of circumstellar clumps formed in massive discs and the exact subset of them migrating down to the central protostar. Other explanations of the formation of circumstellar clumps are plausible, such as the gravitational attraction of gaseous clumps formed within the pre-stellar core or by fragmentation of a neighbouring accretion disc, e.g. during the formation of two massive binaries, and subsequently ejected away by the gravitational sling effect (Vorobyov 2016). In this paper, we continue the interpretation of the clumps' fate. They can lose their envelope and produce accretion-driven events once the material reaches the stellar surface, however, if the clump continues to collapse and does not fall directly to the protostar, it will end up as a close, low-mass companion. An example of a clump having such properties is detailed below.

7.2 Forming close/spectroscopic massive binaries by clump migration

Fig. 15 shows the evolution of the densest grid cell of the clump responsible for the burst happening in Run 1 at 31.4 kyr. We follow its evolution between the times 30.9 and 31.4 kyr. At 31.32 kyr, the core of the clump reaches a density of $\rho \approx 8.6 \times 10^{-11} \text{ g cm}^{-3}$ and $T \approx 1724$ K. About 24 years later, those numbers are $\rho \approx 4.13 \times 10^{-10} \text{ g cm}^{-3}$ and a temperature $T \approx 4638 \gg 2000$ K because no dissociation is included into our equation of state. This is sufficient to consider this clump as to be on its path to star formation, indicating that our simulations are consistent with the formation scenario of a massive binary by disc fragmentation. The central protostar is therefore in an embryonic binary system of a current separation of 10 AU and below when the hot disc fragment disappear into the sink cell, which is much smaller than found in previous calculations (a few 100 AU–1000, see Krumholz et al. 2007b).

Furthermore, given the clump's properties and assuming angular momentum conservation, we estimate at a time 31.36 kyr its centrifugal radius, i.e. the Keplerian orbit at which it falls (see analysis in Meyer et al. 2017). The clump of $M_c \approx 1.2 M_\odot$ is located at a radius of $r = 38$ AU from the protostar, has an azimuthal velocity of $v_\phi \approx 1.8 \times 10^6 \text{ cm s}^{-1}$ and the protostellar mass is $M_\star \approx 16.36 M_\odot$ with a disc mass in the region ≤ 38 AU of $M_d \approx 3.16 M_\odot$. We find that, in the midplane, $R_c = (rv_\phi)^2 / (G(M_\star + M_d)) \approx 27.01$ AU, and 20 years later at a time 31.38 kyr, we find $R_c \approx 4.64 \text{ AU} \approx 996 R_\odot \gg R_\star \approx 100 - 10 R_\odot$. Under our assumptions, it shows that this clump does not directly land onto the protostar as in Meyer et al. (2017). The value of R_c calculated just before the clump enters the sink cell corresponds to a Keplerian period of $P \approx 842$ d which is of the

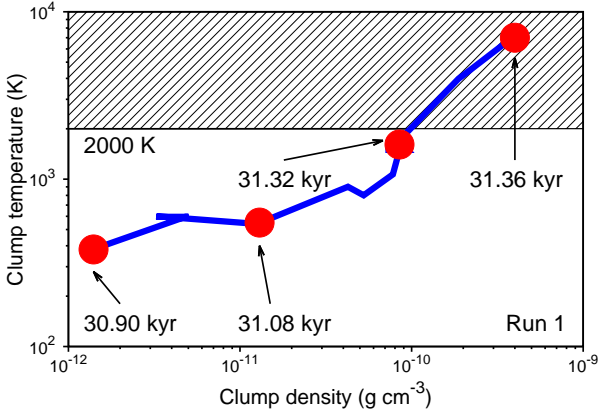


Figure 15. Temperature-density evolution of the circumstellar clump responsible for the first outburst of our Run 1, showing the characteristics of a gaseous blob on the path to low-mass star formation. The hatched region fall under dissociation, not included in our simulations.

order to the period range observed in some massive binaries (Kobulnicky et al. 2014). As discussed in Meyer et al. (2017), this value of R_c is an upper limit because of the clump’s angular momentum loss during its inward migration. Therefore, the corresponding system will be tighter and result in a so-called short-period binary ($P \sim 10 - 100$ d). This naturally evolves towards a massive spectroscopic binary ($P \sim 1 - 10$ d) (Kobulnicky et al. 2014), when the central protostar leaves the pre-main-sequence phase and becomes an O-type star.

7.3 Accretion-driven outbursts from high-mass star-forming regions as tracer of close/spectroscopic massive binary formation

Since envelope and core of the clumps may separate during the infall due to tidal stripping, both phenomenon – accretion-driven outbursts and close binary formation – may happen together, and the bursts would be, in this case, a tracer of close/spectroscopic binary formation. A follow-up study will statistically investigate the properties of the accretion spikes in our simulations, as in Vorobyov & Basu (2015). Although, our study demonstrates its consistency within our assumptions, we nevertheless can not give the definitive proof that close binaries can form by the disc fragmentation in the surroundings of the protostar, since the migration of circumstellar clumps can only be followed up to $r_{in} = 10 \text{ AU} \gg R_*$. Discriminating the fate of the clumps between close binaries and accretion-driven outbursts is difficult since it requires multi-scale simulations resolving at the same time the disc fragmentation at $\sim 100 \text{ AU}$ and the fall of clumps down to $\sim 1000 R_\odot$ for a close/spectroscopic binary, and/or eventually to $\sim 100 R_\odot$ for an accretion burst. Such simulations are far beyond the scope of this work.

8 DISCUSSION

This section is devoted to a general discussion of our results. We review the limitation of our setup, especially in terms of micro-physical processes that we may include into future studies in order to tend towards a more realistic description of the surroundings of massive protostars. We briefly compare our results with previous studies, compare them with results obtained with sink particles methods and we discuss what could influence the fragmentation of

our accretion discs. Finally, we predict what our results would look like when observed.

8.1 Limitation of the model

Despite of reaching sub-AU resolution within the inner region of the accretion discs, our simulations still suffer from a lack of spatial resolution. Increasing the grid resolution would allow us to calculate in more detail, e.g. the internal physics of the migrating circumstellar clumps. This problem equally affects codes with static grids or with mesh-refinement techniques such as FLASH (Banerjee & Pudritz 2007), ORION (Krumholz et al. 2007b) or RAMSES (Commerçon et al. 2010). Although chosen in accordance with current numerical studies on disc fragmentation in star formation, several other assumptions of our method could be subject to further improvements. In addition to the treatment of the radiation itself, it mainly concerns:

(i) The utilised prescription to estimate the accretion luminosity. In Meyer et al. (2017), the accretion luminosity is assumed to be a fraction $f = 1$ of the gravitational potential energy of the material crossing the inner boundary. This fraction is finally converted into stellar radiation instead of being absorbed and mixed to the stellar interiors. Motivated by observations, Offner et al. (2009) constrained this value to $f = 3/4$, that, in our case, will make our accretion spikes less intense. This will change our estimate of the increase in accretion luminosity during the bursts and make our results even more consistent with the observations of Caratti o Garatti et al. (2016), strengthening their interpretation as a manifestation of the burst mode of massive star formation. Complex star-disc interaction simulations calculating in detail the accretion and penetration of disc material into the interior of the protostar in the vein of Kley & Lin (1996) are required to determine f more accurately.

(ii) The initial shape of the pre-stellar core and/or the choice of perturbation seeds for the gravitational instability. We initialize the simulation with spherically-symmetric pre-stellar cores, however, observations have revealed their non-isotropic, filamentary shapes. Particularly, the study on massive star formation of Banerjee et al. (2006) uses initial conditions taken as a turbulent core structure extracted from a previously-calculated cluster-forming clump. The considered symmetry breaking of the gravitational collapse in our case is numerical (cf. Hosokawa et al. 2016), while many studies initially sparse the density field of the pre-stellar core with a particular seed mode ($m=2$, see Banerjee & Pudritz 2007) that is azimuthally imposed on the top of the density profile.

(iii) The stellar motion. The gravitational influence of the disc onto the star is neglected in our setup in which the star is static. The effect of the disc inertia onto the protostar becomes important when discs develop heavy and/or extended spiral arms displacing the barycenter of the star/disc system at radii larger than the size of the sink cell, which in its turn influences the stellar motion. This is intrinsically taken into account in simulations utilizing moving sink particles as representations of forming stars and it will be included in future studies with the method described in Hosokawa et al. (2016) and Regály & Vorobyov (2017). This is a well-known inconvenience of simulations of accretion discs with static central object. Also note that numerical simulations with grid-refinement methods do not strictly conserve angular momentum and suffer from grid-alignment effects. However, since the models of Klassen et al. (2016) do not fragment to the same degree as ours, we conclude that the preponderant issue for disc fragmentation is spatial resolution. Including the stellar motion should make the discs have

net angular momentum that is lower than in the case without stellar motion. The disc will be of smaller radius and then less prone to fragmentation. However, this effect can easily be counterbalanced by a mild increase of the initial rotation rate in the parental cloud, as shown in Regály & Vorobyov (2017).

(iv) Simulation time. The numerical cost of simulations of massive stars like ours is huge and currently obliges investigations to be restricted to the early formation phase. However, since long-term evolution simulation of low-mass star formation (Matsumoto et al. 2017) highlighted that, under some circumstances, discs modify their shape and orientation, one can wonder whether totally new disc morphologies will arise around more evolved young high-mass stars.

(v) Missing physical mechanisms. Apart from covering the parameter space which is still far from being fully explored in terms of initial pre-stellar core mass M_c , size R_c and ratio of kinetic per gravitational energy β , neglected microphysical processes may also change our results. Particularly, the ionization feedback of the protostar filling the bipolar outflows which develops perpendicular to the discs and giving birth to bipolar H II regions that can be observed (Campbell 1984), may experience intermittency (Tanaka et al. 2017) as in primordial star formation (see Hosokawa et al. 2016). Thus, the inclusion of the magnetization of the pre-stellar core is also necessary to tend towards a global picture of star formation because it influences at the same time the jet morphology (Pudritz et al. 2007; Frank et al. 2014) and the fragmentation of accretion discs (Hennebelle et al. 2016; Fontani et al. 2016), see Section 8.4.

(vi) The midplane-symmetric nature of our simulations. This can be improved by considering the full three-dimensional evolution of the protostellar disc. We force the disc to develop symmetrically with respect to the plane normal to the rotation axis, see Fig. 4. Full “ 4π ” models would allow us to take into account the vertical bending of the disc visible, for example in Fig. 13 of Krumholz et al. (2007b). Note also, that, if our simulations with static stars do not allow us to appreciate the effects of the disc wobbling, models with Cartesian grids cannot qualitatively pronounce on the absence of stellar motion on the disc dynamics. For all those reasons, the assumptions of midplane-symmetry of our simulations are reasonable and our method does not overestimate fragmentation from this point of view. What causes disc bending modes and how that can affect disc fragmentation deserves a separate focused study.

(vii) The size of the sink cell. Indeed, our method neglects the fate of the clumps once they cross the innermost boundary of 10 AU (see also Meyer et al. 2017), which has so far not been modeled up to the boundary layer of the disc. The presence in the close environment of protostars of more (smaller) clumps in chaotic and mutual interaction would change the geometry of the accretion flow onto the protostar, that are influenced by complex radiation processes, such as the line-ablation mechanisms acting in the surroundings of O/Be stars (Kee et al. 2016). However, studies devoted to low-mass star formation demonstrated that while about half of the clumps are gravitationally supported and remain in the disc, the falling clumps may be ejected from the disc or further fragment within the innermost disc regions (Greif et al. 2012; Meru 2015; Vorobyov 2016). This may be enhanced by H_2 cooling and collisional emission, not treated in our simulations.

However, such improvements would only be possible at the cost of even more computationally-intensive simulations requiring higher spatial resolution and huge memory resources. Particularly, this will give us access to the probable chaotic behaviour of the

circumstellar clumps in the inner region of the disc (see discussion in Meyer et al. 2017).

8.2 General discussion

The study of low-mass star formation has led to a large literature on its theory, but the three-dimensional modelling of the birth of high-mass stars is still a relatively recent field of research. A few works only tackled the problem and their differences principally lie in the way to treat the stellar feedback and/or in the choice of pre-stellar core initial configuration. Most simulations assume a density distribution $\rho(r) \propto r^{-3/2}$ but models such as in Kuiper et al. (2011) and Kuiper & Yorke (2013a) additionally consider $\rho(r) \propto r^{-2}$. The other fundamental parameter of the pre-stellar core is its initial velocity field. While some studies considered non-rotating pre-stellar environments in which turbulence was initially driven (Krumholz et al. 2007b), non-solid body rotating pre-stellar cores have begun to be investigated in Meyer et al. (2017) with $\Omega(R) \propto R^{-0.75}$ and our work continues this with $\Omega(R) \propto R^{-0.35}$. The initial mass of pre-stellar cores is typically taken to $M_c \approx 100 M_\odot$ and the ratio of rotational-to-gravitational energy to $\beta \approx \text{few } \%$ as in our study, but models have been calculated with $M_c = 1000 M_\odot$ (Peters et al. 2010) and $\beta \geq 10\%$ (Seifried et al. 2011; Klassen et al. 2016). A more detailed review of the initial conditions of the pre-stellar cores in terms of M_c and β -ratio can be found in Meyer et al. (2017).

The manner of treatment of radiation feedback differs greatly from study to study. Pre-calculated cooling curves are less accurate but allow the coverage of large parameter spaces (Banerjee & Pudritz 2007; Seifried et al. 2011), e.g. including the magnetization of turbulent pre-stellar cores (Seifried et al. 2013), whereas radiation transport algorithms taking into account the physics of dust are able to self-consistently model the dust sublimation front (Kuiper et al. 2010). Our method is a modification of the PLUTO code (Mignone et al. 2007, 2012) described in Kuiper et al. (2010, 2011). Recently, a similar scheme has been implemented into the FLASH and ORION codes, using a mesh-refinement grid (Klassen et al. 2014; Rosen et al. 2017). In that sense, our study has the advantage to have a highly-resolved grid in the inner parts of the disc together with a radiative transfer solver more accurate than a simple cooling law, but it has the disadvantage not to properly resolve clumps potentially forming at larger radii. Although the frequency-dependent ray-tracing method has been successfully benchmarked with respect to our utilised grey solver (Kuiper & Klessen 2013), its requirement in terms of numerical resources was too high. However, radiation transport methods making use of a frequency-dependent ray-tracing solver have been developed and used in the context of three-dimensional massive star formation simulations (Kuiper et al. 2011; Rosen et al. 2016). Particularly, the effects of the interplay between such radiation transport methods and grid resolution on the modelling of (Rayleigh-Taylor unstable) bipolar outflows from massive stars is largely discussed in Kuiper et al. (2012), in Rosen et al. (2016) and in Harries et al. (2017).

Another similarity between our simulations and recent studies is their consistency with respect to analytical criteria predicting disc fragmentation. Numerical solutions of the surroundings of high-mass protostars is typically compared to the Toomre, Gammie and Hill criteria. As for other kind of self-gravitating discs, the Toomre criterion characterise well fragmenting regions ($Q \leq 0.6$, see Takahashi et al. 2016; Klassen et al. 2016) whereas the Gammie analysis alone is in most regions fulfilled and therefore not sufficient to discriminate between fragmenting and non-fragmenting

scenario, e.g. at the early stage of the disc formation. Additionally, accordance between numerical simulations and the Hill analytic prediction were found. It applies to our unstable models as it did in the disc simulations of Klassen et al. (2016) that are stable to fragmentation, but unstable to development of spiral modes. Consequently, this criterion is the most reliable tool so far to characterize the stability of spiral arms in discs from young stars.

Fragmentation as a response of accretion discs against gravitational instability has been widely investigated analytically and numerically in different astrophysical contexts. Particularly, the study of Kratter & Matzner (2006) considers the antagonistic effects of both angular momentum transport, leading discs to fragmentation and viscous heating tending to stabilize them. Under those assumptions which “underestimate the prevalence of disc fragmentation”, they found that discs around high-mass stars ($\geq 10 M_{\odot}$) are prone to fragmentation and that this probability increases with M_{*} . Our Run 1 with solid-body rotation is consistent with such prediction since the disc fragments at a time ≈ 30 kyr when the protostar has reached $\approx 17 M_{\odot}$, see Fig. 1c and Fig. 5a). However, our disc models initially deviating from rigid rotation fragment before the protostar reaches such mass, e.g. at a time ≈ 30 kyr when the central protostar is only $\approx 7 M_{\odot}$ (Run 2, see Fig. 2b and Fig. 5b). Finally, we recall that the episodic feedback of secondary objects have been shown to play a role in further enhancing disc fragmentation shortly after accretion driven-outbursts (Mercer & Stamatellos 2016). This process may apply to our discs around massive protostars and further enhance their fragmentation (see Section 8.3).

8.3 Self-consistent versus sink particle simulations

The sink particle approach consists in coupling a discrete N-body-like method to a continuous resolution of the hydrodynamics equations in a grid-based code. Therefore, it is a violation of the self-consistent treatment of the different physical processes at work in the computational domain. Such approach is nevertheless unavoidable, since low-mass stars such as brown dwarfs or solar-type stars appear as point-mass objects, once they undergo second collapse from first hydrostatic cores down to stellar densities. All the subtlety lies in (i) applying sufficiently strong sink-creation criteria in order to avoid fictitious particle formation leading to overestimating the number of stars and (ii) introducing them as late as possible during the secondary gravitational collapse, ideally when the grid size is of the order of the radius of the new-born star, not to artificially influence the local protostellar disc dynamics. Indeed, introducing sinks modifies the gas dynamics, itself a function of the resolution of the simulation at the moment of the particle creation.

Criteria allowing codes to generate sinks greatly vary between numerical schemes and simulations. A too sophisticated but very realistic particle-creation algorithm will rarely secondary star formation, leading to the conclusion of disc stability, despite of a Q - and β -unstable disc (Klassen et al. 2016), whereas a simplified one will produce over-numerous and unphysical star formation. Indeed, Rosen et al. (2016) notes that “multiplicity results are sensitive to the physics included, radiative transfer treatment used, and sink creation and merging criteria employed”. Moreover, choosing a (set of) criterion(s) for sink particles creation is equivalent to a preference for particular star formation laws, still largely under debate. Particularly, Machida et al. (2014) showed with non-turbulent, (non-)ideal magnetohydrodynamics simulations of rotating Bonnor–Ebert spheres of initial mass ranging from 1.0 to $100 M_{\odot}$, how sensitive disc solutions around low- and high-mass stars can be as a function of both the accretion radius of sink par-

ticles and the density threshold constituting their principal creation condition (see also discussion in Padoan & Nordlund 2011). They concluded on the necessity of sink accretion radius ≤ 1.0 AU and a sink particle density threshold $\geq 10^{13} \text{ cm}^{-3} \simeq 10^{-11} \text{ g cm}^{-3}$. The properties of the companion core in Fig. 15 is consistent with this assertion, however, one can clearly see that our clump becomes a star when its core is denser than $10^{-10} \text{ g cm}^{-3}$, revealing (at least in this case) the insufficiency of the criterion of Machida et al. (2014) since our gaseous clump is not yet hot enough to be considered as a secondary star. Perhaps a more reliable criterion for sink particle creation could be the temperature of the clump’s core? Also pointed by Hennebelle et al. (2011), the “use of sinks may alter significantly the evolution of the calculations in particular in the presence of magnetic field”, which is an additional drawback of numerical models like in Myers et al. (2013, 2014).

Our method gets rid of those caveats since the local collapse is self-consistently captured in the density and temperature fields. We justify the use of a spherical coordinate system by our scientific goal, which is to understand the formation of spectroscopic companions to massive OB stars, by exploring star formation and migration in the inner part of the disc. The main caveat of our disc dynamics is therefore the lack of spatial resolution in their outer region. However, as discussed in Section 5, this is acceptable since the migrating clumps develop in the inner and intermediate region of the protostellar disc. Our alternative method to simulations with Cartesian grids and sink particles self-consistently produce discs fragmenting into clumps hot enough to verify the condition of secondary star formation, which is a confirmation of the discovery of multiplicity in the massive protostellar context in Krumholz et al. (2007b). With both methods, the number of companions forming in the disc decreases with the consideration of the pre-stellar core’s magnetization (Machida et al. 2014; Commerçon et al. 2011), see also Section 8.4. No formation of twin massive binaries (Krumholz et al. 2009a) is observed directly in our models, although Run 3 shows the formation of a massive disc-like clump (Fig. 3).

In the case of models with “smart” particles possessing their own feedback, high numerical resolution is needed to resolve the accretion discs around the formed secondary stars, in which the complex flow induces accretion rate variability and makes the feedback of the secondary stars episodic by the mechanisms largely described in Vorobyov & Basu (2010) and Bae et al. (2014). This will subsequently affect the results by further favouring violent fragmentation of the discs (see Mercer & Stamatellos 2016). Even more realistic sink particles should take into account jet-launching mechanisms perturbing the disc dynamics by creating disc cavities or outflows, and/or, in the case of, e.g. intermediate-mass secondary star formation (Reiter et al. 2017). Located beyond the dust sublimation radius, their H II region will intermittently release ionized gas into the radiation-shielded part of the central protostar’s disc and enrich it with momentum and energy, perturbing its internal thermodynamics.

8.4 What can we expect on disc fragmentation by improving on the limitations of the models?

With the help of a grid more resolved in the stellar close environment than ever before, Meyer et al. (2017) revealed the fragmenting character of circumstellar discs. Since our models showed the clump-forming nature of discs around massive stars, one may ask, whether additional physical effects, not resolved in our simulations may arise and change the global picture of our solutions? As an example, increasing the spatial resolution in low-mass star forma-

tion simulations enhanced the possibility of circumstellar clumps to be ejected out of their host accretion disc (Vorobyov 2016). High-resolution studies in the context of low-mass and primordial star formation have also shown that further fragmentation may take place in the very innermost disc regions modelled by our static sink cell. Those phenomena are provoked by migrating falling fragments or by H_2 cooling and/or by collisionally induced emission, see Stacy et al. (2010); Greif et al. (2012) but also Meru (2015), however, they did not suppress physical conclusions that were previously drawn in their respective context. Therefore, the same may apply in the massive protostellar context.

Higher resolution simulations may highlight other detailed features in the fragmentation dynamics such as very inner accretion disc fragmentation occurs during massive star formation. This will therefore result in a pattern of very small gaseous clumps that can merge together, orbit on to the central protostar or be dynamically ejected away by gravitational sling, revealing amongst other clump-clump interactions as those discussed in detail in Zhu et al. (2012). Although this would change the geometry of the accretion and affect the detailed variability of the protostellar luminosity, the trajectory heavy clumps such ours that migrate fast, hosting the birth of a secondary star, will not be greatly perturbed. They will either fall directly onto the stellar surface (accretion burst), orbit around it (close binary formation) or lose their envelope while reaching a Keplerian orbit around the central protostar (close binary formation accompanied by accretion-driven event). One should also keep in mind that such criticisms are also valid regardless the used coordinate system, the grid refinement criteria and/or the utilised sink particles creation algorithms. Cartesian simulations of massive star formation like in, e.g. Krumholz et al. (2007b) or Klassen et al. (2016), but allowing more grid refinement levels and/or comparing different sink-particle algorithms are therefore highly desirable.

The above discussion refers to the aggravation of fragmentation once it has been triggered in the core, however, some physical processes can directly influence the fragmentation by modifying the disc temperature. Two other processes can indeed, under some circumstances, directly control whether fragmentation itself occurs, namely the presence of magnetic fields and/or the initial turbulence of the pre-stellar core. Often neglected for the sake of simplicity, the magnetization of the gravitationally collapsing structures can modify the disc dynamics. This has been reported at different length scales, spanning from giant molecular clouds to low-mass star-producing cores (Commerçon et al. 2010; Tomida et al. 2010). The effects of the pre-stellar core magnetic properties on delaying, promoting, or preventing disc fragmentation, together with a description of the variety of the forming different low-mass binaries systems are discussed in Tomida et al. (2015). Particularly, the interplay between the magnetic breaking of the infalling gas and the radiative feedback of the protostar can inhibit the initial fragmentation processes of collapsing pre-stellar cores. Note that this applies to the regime of a strong magnetic field strength (Commerçon et al. 2011) under which our results do not fall as we neglect magnetization.

These magnetized models in the study of Commerçon et al. (2011) propose a channel to generate isolated O stars. However, it also underlines that two secondary fragments "associated with a relatively high Jeans mass reservoir" form, and consequently one could expect "this early fragmented system [to] give rise to a close massive binary system". Such conclusions were beforehand only drawn by Lagrangian particles simulations of Bonnell & Bate (2005) and by the hydrodynamical disc fragmentation model of Krumholz et al. (2009b). Although using two totally different

methods, they both demonstrate the possibility of producing twin massive binaries by pre-stellar core gravitational collapse followed by disc fragmentation, under the assumption of a neglected magnetization of the gas. Finally, note that since star-forming regions are dense, the non-ideal character of magneto-hydrodynamical processes such as Ohmic dissipation, Hall effect and ambipolar diffusion can, as an additional effect, influence the gas dynamics. Their significance on the physics of interstellar filaments (Ntormousi et al. 2016) and on low-mass star formation (Masson et al. 2012; Tomida et al. 2015; Masson et al. 2016; Marchand et al. 2016) implies that they, no doubt, should impact high-mass star formation as well.

Turbulence is another key ingredient in the theoretical determination of star formation rates (Hennebelle & Chabrier 2011). In the case of the gravitational collapse of a single, isolated pre-stellar cloud, turbulence modifies the gravitational collapse itself but also directly affects its magnetization. Particularly, it has been suggested that the so-called magnetic breaking catastrophe is a natural consequence of the over-idealized initial conditions of low-mass star formation simulations, and that native pre-stellar turbulence naturally leads to Keplerian disc formation (Seifried et al. 2012), although the work of Wurster et al. (2016) brings a non-ideal but non-turbulent solution to this problem. Additionally, turbulence strongly influences the pre-stellar core magnetic field coherence (Seifried et al. 2015). The study of Rosen et al. (2016) includes simulations with stellar radiation and turbulent initial conditions which evolve towards complete disorganization of the disc-bubble system in the protostellar surroundings. As Keplerian discs (Johnston et al. 2015) and clear disc-outflow structures (Zinchenko et al. 2015) have been observed around young high-mass stars, those models indicate that other feedback processes stabilizing the pressure-driven radiative bubble such as outflow launching mechanisms (Kuiper et al. 2015, 2016) must be at work efficiently during the formation of massive stars. Since sub-AU-resolved, three-dimensional gravitation-radiation-magnetohydrodynamic, turbulent simulations of high-mass star formation have not been conducted yet, the question is therefore to know by how much fragmentation in the context of our pre-stellar cores would be affected if considered with both (non-ideal) magnetization and turbulence. Those questions will be addressed in a subsequent study.

8.5 Prediction of observed emission

Although observational evidences for bipolar $H II$ regions (Franco-Hernández & Rodríguez 2004) and accretion flows (Keto & Wood 2006) around young high-mass stars became more numerous over the past years, the direct imaging of their accretion discs was until recently under debate (Beuther et al. 2012), mostly because of the high opacity of the parent environment in which they form and large distances to these objects (Zinnecker & Yorke 2007). Recent observations from the *ALMA* interferometer suggested the presence of a Keplerian accretion disc in the surroundings of the early O-type star AFGL 4176 (Johnston et al. 2015). Similar techniques revealed the presence of a clumpy gaseous disc-like structure around the young high-mass stellar object of the S255IR area (Zinchenko et al. 2015) which is associated to a FU Orionis-like outburst (Burns et al. 2016; Caratti o Garatti et al. 2016). An equivalent discovery around the young early massive star G11.920.61 MM1 has been reported using the velocity gradient of compact molecular line emission oriented perpendicularly to a bipolar molecular outflow in Ilee et al. (2016) and the number of young massive candidates surrounded by

a self-gravitating disc increases (Forgan et al. 2016). Several ongoing observational campaigns currently aim at detecting signs of disc fragmentation, e.g. with the *ALMA* facility (Cesaroni et al. 2017, in press).

To appreciate our results in the context of observations, we perform a dust continuum radiative transfer calculation with the code *RADMC-3D*¹ (Dullemond 2012) using a Laor & Draine (1993) dust mixture based of Silicates crystals with density and temperature distributions are directly imported from our simulations. Fig. 16 shows a synthetic 1.2mm dust continuum emission of our Run 1 at a time ≈ 40 kyr, viewed under an inclination angle of 30° . The protostellar mass is $\approx 25 M_\odot$ which corresponds to AFGL 4176's constrained mass, however, the disc mass is $\approx 30 M_\odot$ which is larger than the $12 M_\odot$ used to fit the properties of AFGL 4176. The radius of the disc of ≈ 2 kAU is consistent with the observations. We assumed the protostar to be a black body source of effective temperature directly given by the stellar evolution routine of the simulation $T_{\text{eff}} \approx 37500$ K and of bolometric luminosity $L \approx 85500 L_\odot$ from which photon packages are ray-traced through the accretion disc. The calculations are further post-processed with the *SIMOBserve* and *CLEAN* tasks of the *Common Astronomy Software Applications*² (*CASA*, McMullin et al. 2007) to produce synthetic *ALMA* observations of our disc as if located at the coordinates of AFGL 4176. Telescope parameters are chosen to be the configuration 4.9 for Cycle 4 *ALMA* observations, with a bandwidth of 1.8 GHz with ≈ 3 hours of integration time. The central frequency of the combined continuum emission is 249.827 GHz (1.2 mm) and imaging was carried out using Briggs weighting with a robust parameter of 0.5. Under those assumptions and parameters, our *ALMA* rendering of Run 1 that is shown in Fig. 16 has observable emission. It presents the typical structure of an accretion disc around with spiral arms and clumpy substructures in it. A more detailed analysis of the molecular surroundings of this model, including line emission, is left for future work (Johnston et al., in prep).

9 CONCLUSION

We have run three-dimensional gravito-radiation-hydro simulations of the collapse of $100 M_\odot$ pre-stellar cores rotating with a kinetic-to-gravitational energy ratio of $\beta = 4\%$ and with different initial conditions in terms of initial angular momentum distribution, in the context of a non-magnetized disc generated by an initially non-turbulent pre-stellar core. We perform the simulations during at least ≈ 35 kyr to generate protostars of ≈ 18 to $35 M_\odot$. Our state-of-the-art treatment of the stellar radiation feedback, together with the sub-AU spatial resolution of the inner region of the accretion disc allow us to realistically follow the evolution of the circumstellar medium of the early high-mass stars. We have investigated the stabilizing role of the direct stellar irradiation and performed a resolution study, ensuring that disc gravitational fragmentation accounts for the central protostellar feedback and/or artificially triggered. All our models have accretion discs whose spiral arms fragments by gravitational instability into a pattern of gaseous clumps, while continuously feeding the central protostars at highly variable accretion rates of $\sim 10^{-4} - 10^{-3} M_\odot \text{ yr}^{-1}$. As in the other regimes of star formation (see Smith et al. 2012; Vorobyov et al.

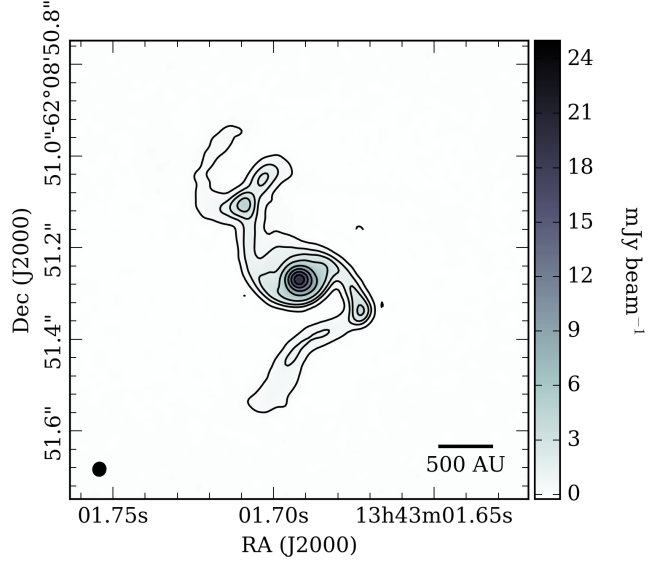


Figure 16. Dust continuum *ALMA* prediction of our Run 1 in the context of the young high-mass stars AFGL 4176 (Johnston et al. 2015). We consider a snapshot from the model at a time 40.0 kyr, when the protostar has reached $24.5 M_\odot$. The overall disc and its brightest circumstellar clumps have a radius 2 kAU and $\approx 0.6 - 1.0$ kAU from the protostar, respectively. Image intensity is in mJy/beam.

2013; Vorobyov & Basu 2015, and references therein), those circumstellar clumps episodically generate luminous accretion-driven outbursts when migrating down onto the protostar. Our study shows that the mechanism introduced in Meyer et al. (2017) also happens for the different rotation profiles investigated herein.

Particularly, those flares are similar to the FU-Orionis-like episodic accretion-driven outbursts observed in the young high-mass stellar system S255IR-SMA1 (Burns et al. 2016; Caratti o Garatti et al. 2016). Some gaseous clumps migrate to the close surroundings (≤ 10 AU) of the central protostar while simultaneously experiencing an increase of their central density and temperature that can reach up to $\approx 10^{-8} \text{ g cm}^{-3}$ and ≥ 2000 K, respectively. The clumps are sufficiently massive ($\approx 0.5 - \text{a few } M_\odot$) and their core is hot and dense enough to be considered as being on the path to the second gravitational collapse down to stellar densities. We show that such nascent companions can fast-migrate down to the central protostar, constituting a massive binary system, made of a massive component plus a low-mass companion in close Keplerian orbit around it. We conclude on the viability of the disc fragmentation channel to explain the formation of close massive proto-binaries made of a young high-mass component and at least a low mass companion, which are the progenitors of the future post-main-sequence spectroscopic massive binaries (see also Sana et al. 2012; Mahy et al. 2013; Kobulnicky et al. 2014, for an observational study of close-orbit, O-star-involving massive binary statistics). We underline that disc fragmentation, high variations of the protostellar accretion rate, episodic accretion-driven outbursts and close binary formation are tightly correlated mechanisms, and we predict that both phenomena can happen together. Consequently, luminous outbursts from young massive stars are the signature of the presence of its surrounding accretion disc, a tracer of the migration of circumstellar disc fragments but may also be at the same time a signature of the formation of close companions that will become the spectroscopic companions of a future O-type star.

¹ <http://www.ita.uni-heidelberg.de/~dullemond/software/radmc-3d/>

² <https://casa.nrao.edu/>

We test our accretion discs against several semi-analytical criteria characterising the fragmentation of self-gravitating discs. We find that our discs are consistent with the so-called Toomre, Gammie and Hill criteria, which is consistent with the analysis presented in Klassen et al. (2016), which we can summarise as follows: the Gammie criterion is fulfilled by our discs while the Toomre criterion alone allows us to discriminate fragmenting from non-fragmenting accretion discs ($Q \leq 0.6$, see Takahashi et al. 2016). The Hill criterion, even applied to the early formation phase of our discs, predicts their subsequent evolution with respect to fragmentation. Radiative transfer calculations against dust opacity in the context of the Keplerian disc surrounding the young high-mass star AFGL-4176 (Johnston et al. 2015) indicate that clumps in our disc models are detectable with *ALMA*. Such disc fragments should be searched with modern facilities such as *ALMA* or the future *European Extremely Large Telescope (E-ELT)* within high-mass star formation regions from which strong maser emission or evidence of accretion flows have been recorded, e.g. W51 (Keto & Klaassen 2008; Zapata et al. 2009) and W75 (Carrasco-González et al. 2015).

This work highlights the need for highly spatially resolved simulations of massive star formation simulations as an additional issue to numerical methods and physical processes. It further stresses the challenging character of numerical studies devoted to the surrounding of young hot stars, as well as the similarities between massive star formation mechanisms (accretion variability and disc fragmentation) with the other (low- and primordial-) mass regimes of star formation. Our work, showing a possible pathway for the formation of spectroscopic massive binaries, will be continued and expanded to obtain a deeper understanding of the circumstellar medium of young massive stars and the implications for massive stellar evolution. Follow-up studies will investigate the effects of several physical processes which we have so far neglected, such as the inertia of the protostar, its ionizing feedback or the magnetization of the pre-stellar core. This should allow us to pronounce more in detail the effects of disc fragmentation around early protostars as a function of the initial properties of their pre-stellar cores.

ACKNOWLEDGEMENTS

The authors thank the anonymous referee for their useful advice and suggestions which greatly improved the manuscript. D. M.-A. Meyer and E. Vorobyov thank B. Stecklum for his invitation at Thüringer Landessternwarte Tautenburg. This study was conducted within the Emmy Noether research group on "Accretion Flows and Feedback in Realistic Models of Massive Star Formation" funded by the German Research Foundation under grant no. KU 2849/3-1. E. I. Vorobyov acknowledges support from the Austrian Science Fund (FWF) under research grant I2549-N27. The authors gratefully acknowledge the computing time provided on the bwGrid cluster Tübingen. and on the ForHLR I cluster at the Steinbuch Center for Computing Karlsruhe. This research has made use of Astropy, a community-developed core Python package for Astronomy (Astropy Collaboration, 2013) and of SAOImage DS9.

REFERENCES

- Bae J., Hartmann L., Zhu Z., Nelson R. P., 2014, *ApJ*, 795, 61
 Banerjee R., Pudritz R. E., 2006, *ApJ*, 641, 949
 Banerjee R., Pudritz R. E., 2007, *ApJ*, 660, 479
 Banerjee R., Pudritz R. E., Anderson D. W., 2006, *MNRAS*, 373, 1091
 Banerjee R., Pudritz R. E., Holmes L., 2004, *MNRAS*, 355, 248
 Bergin E. A., Tafalla M., 2007, *ARA&A*, 45, 339
 Beuther H., Linz H., Henning T., 2012, *A&A*, 543, A88
 Beuther H., Ragan S. E., Johnston K., Henning T., Hacar A., Kainulainen J. T., 2015, *A&A*, 584, A67
 Bonnell I. A., Bate M. R., 1994, *MNRAS*, 271
 Bonnell I. A., Bate M. R., 2005, *MNRAS*, 362, 915
 Bonnell I. A., Bate M. R., Zinnecker H., 1998, *MNRAS*, 298, 93
 Boss A. P., 2017, *ArXiv e-prints*
 Burns R. A., Handa T., Nagayama T., Sunada K., Omodaka T., 2016, *MNRAS*, 460, 283
 Campbell B., 1984, *ApJ*, 282, L27
 Caratti o Garatti A., Stecklum B., Garcia Lopez R., Eisloffel J., Ray T. P., Sanna A., Cesaroni R., Walmsley C. M., Oudmaijer R. D., de Wit W. J., Moscadelli L., Greiner J., Krabbe A., Fischer C., Klein R., Ibanez J. M., 2016, *Nature*, pp 1745–2481
 Carrasco-González C., Torrelles J. M., Cantó J., Curiel S., Surcis G., Vlemmings W. H. T., van Langevelde H. J., Goddi C., Anglada G., Kim S.-W., Kim J.-S., Gómez J. F., 2015, *Science*, 348, 114
 Cesaroni R., Galli D., Lodato G., Walmsley M., Zhang Q., 2006, *Nature*, 444, 703
 Cesaroni R., Hofner P., Araya E., Kurtz S., 2010, *A&A*, 509, A50
 Clarke C. J., Harper-Clark E., Lodato G., 2007, *MNRAS*, 381, 1543
 Commerçon B., Hennebelle P., Audit E., Chabrier G., Teyssier R., 2010, *A&A*, 510, L3
 Commerçon B., Hennebelle P., Henning T., 2011, *ApJ*, 742, L9
 Dessart L., Langer N., Petrovic J., 2003, *A&A*, 404, 991
 Dullemond C. P., 2012, *RADMC-3D: A multi-purpose radiative transfer tool*, Astrophysics Source Code Library
 Durisen R. H., Boss A. P., Mayer L., Nelson A. F., Quinn T., Rice W. K. M., 2007, *Protostars and Planets V*, pp 607–622
 Evans II N. J., 1999, *ARA&A*, 37, 311
 Federrath C., Banerjee R., Clark P. C., Klessen R. S., 2010, *ApJ*, 713, 269
 Fendt C., 2011, *ApJ*, 737, 43
 Fendt C., Sheikhezami S., 2013, *ApJ*, 774, 12
 Flaig M., Ruoff P., Kley W., Kissmann R., 2012, *MNRAS*, 420, 2419
 Fontani F., Commerçon B., Giannetti A., Beltrán M. T., Sánchez-Monge A., Testi L., Brand J., Caselli P., Cesaroni R., Dodson R., Longmore S., Rioja M., Tan J. C., Walmsley C. M., 2016, *A&A*, 593, L14
 Forgan D., Rice K., 2012, *MNRAS*, 420, 299
 Forgan D., Rice K., Cossins P., Lodato G., 2011, *MNRAS*, 410, 994
 Forgan D. H., Ilee J. D., Cyganowski C. J., Brogan C. L., Hunter T. R., 2016, *MNRAS*, 463, 957
 Franco-Hernández R., Rodríguez L. F., 2004, *ApJ*, 604, L105
 Frank A., Ray T. P., Cabrit S., Hartigan P., Arce H. G., Bacciotti F., Bally J., Benisty M., Eisloffel J., Güdel M., Lebedev S., Nisini B., Raga A., 2014, *Protostars and Planets VI*, pp 451–474
 Fuente A., Neri R., Martín-Pintado J., Bachiller R., Rodríguez-Franco A., Palla F., 2001, *A&A*, 366, 873
 Gammie C. F., 1996, *ApJ*, 462, 725
 Greif T. H., Bromm V., Clark P. C., Glover S. C. O., Smith R. J., Klessen R. S., Yoshida N., Springel V., 2012, *MNRAS*, 424, 399
 Greif T. H., Springel V., White S. D. M., Glover S. C. O., Clark P. C., Smith R. J., Klessen R. S., Bromm V., 2011, *ApJ*, 737, 75
 Haemmerlé L., Eggenberger P., Meynet G., Maeder A., Charbonnel C., 2016, *A&A*, 585, A65
 Haemmerlé L., Eggenberger P., Meynet G., Maeder A., Charbonnel C., Klessen R. S., 2017, *A&A*, 602, A17
 Harries T. J., 2015, *MNRAS*, 448, 3156
 Harries T. J., Douglas T. A., Ali A., 2017, *ArXiv e-prints*
 Hawley J. F., Balbus S. A., 1992, *ApJ*, 400, 595
 Hennebelle P., Chabrier G., 2011, *ApJ*, 743, L29
 Hennebelle P., Commerçon B., Chabrier G., Marchand P., 2016, *ApJ*, 830, L8
 Hennebelle P., Commerçon B., Joos M., Klessen R. S., Krumholz M., Tan J. C., Teyssier R., 2011, *A&A*, 528, A72
 Hosokawa T., Hirano S., Kuiper R., Yorke H. W., Omukai K., Yoshida N., 2016, *ApJ*, 824, 119
 Hosokawa T., Omukai K., 2009, *ApJ*, 691, 823

- Hunter T. R., Brogan C. L., MacLeod G., Cyganowski C. J., Chandler C. J., Chibueze J. O., Friesen R., Indebetouw R., Thesner C., Young K. H., 2017, *ArXiv e-prints*
- Ilee J. D., Cyganowski C. J., Nazari P., Hunter T. R., Brogan C. L., Forgan D. H., Zhang Q., 2016, *MNRAS*, 462, 4386
- Isella A., Natta A., 2005, *A&A*, 438, 899
- Johnston K. G., Robitaille T. P., Beuther H., Linz H., Boley P., Kuiper R., Keto E., Hoare M. G., van Boekel R., 2015, *ApJ*, 813, L19
- Kee N. D., Owocki S., Sundqvist J. O., 2016, *MNRAS*, 458, 2323
- Kessel O., Yorke H. W., Richling S., 1998, *A&A*, 337, 832
- Keto E., Klaassen P., 2008, *ApJ*, 678, L109
- Keto E., Wood K., 2006, *ApJ*, 637, 850
- Klahr H., 2004, *ApJ*, 606, 1070
- Klahr H. H., Bodenheimer P., 2003, *ApJ*, 582, 869
- Klassen M., Kuiper R., Pudritz R. E., Peters T., Banerjee R., Bunttemeyer L., 2014, *ApJ*, 797, 4
- Klassen M., Pudritz R. E., Kuiper R., Peters T., Banerjee R., 2016, *ApJ*, 823, 28
- Kley W., Lin D. N. C., 1996, *ApJ*, 461, 933
- Kobulnicky H. A., Kiminki D. C., Lundquist M. J., Burke J., Chapman J., Keller E., Lester K., Rolan E. K., Topel E., Bhattacharjee A., Smullen R. A., Vargas Álvarez C. A., Runnoe J. C., Dale D. A., Brotherton M. M., 2014, *ApJS*, 213, 34
- Kratter K. M., Matzner C. D., 2006, *MNRAS*, 373, 1563
- Kratter K. M., Matzner C. D., Krumholz M. R., Klein R. I., 2010, *ApJ*, 708, 1585
- Kraus S., Kluska J., Kreplin A., Bate M., Harries T. J., Hofmann K.-H., Hone E., Monnier J. D., Weigelt G., Anugu A., de Wit W. J., Wittkowski M., 2017, *ApJ*, 835, L5
- Krumholz M. R., Klein R. I., McKee C. F., 2007a, *ApJ*, 665, 478
- Krumholz M. R., Klein R. I., McKee C. F., 2007b, *ApJ*, 656, 959
- Krumholz M. R., Klein R. I., McKee C. F., Offner S. S. R., Cunningham A. J., 2009a, *Science*, 323, 754
- Krumholz M. R., Klein R. I., McKee C. F., Offner S. S. R., Cunningham A. J., 2009b, *Science*, 323, 754
- Kuiper R., Klahr H., Beuther H., Henning T., 2010, *ApJ*, 722, 1556
- Kuiper R., Klahr H., Beuther H., Henning T., 2011, *ApJ*, 732, 20
- Kuiper R., Klahr H., Beuther H., Henning T., 2012, *A&A*, 537, A122
- Kuiper R., Klahr H., Dullemond C., Kley W., Henning T., 2010, *A&A*, 511, A81
- Kuiper R., Klessen R. S., 2013, *A&A*, 555, A7
- Kuiper R., Turner N. J., Yorke H. W., 2016, *ApJ*, 832, 40
- Kuiper R., Yorke H. W., 2013a, *ApJ*, 763, 104
- Kuiper R., Yorke H. W., 2013b, *ApJ*, 772, 61
- Kuiper R., Yorke H. W., Turner N. J., 2015, *ApJ*, 800, 86
- Langer N., 2012, *ARA&A*, 50, 107
- Laor A., Draine B. T., 1993, *ApJ*, 402, 441
- Lichtenberg T., Schleicher D. R. G., 2015, *A&A*, 579, A32
- Lin D. N. C., Papaloizou J. C. B., Kley W., 1993, *ApJ*, 416, 689
- Lodato G., 2007, *Nuovo Cimento Rivista Serie*, 30
- Lodato G., Clarke C. J., 2011, *MNRAS*, 413, 2735
- Machida M. N., Hosokawa T., 2013, *MNRAS*, 431, 1719
- Machida M. N., Inutsuka S.-i., Matsumoto T., 2011, *ApJ*, 729, 42
- Machida M. N., Inutsuka S.-i., Matsumoto T., 2014, *MNRAS*, 438, 2278
- Machida M. N., Nakamura T., 2015, *MNRAS*, 448, 1405
- Mahy L., Rauw G., De Becker M., Eenens P., Flores C. A., 2013, *A&A*, 550, A27
- Marchand P., Masson J., Chabrier G., Hennebelle P., Commerçon B., Vaytet N., 2016, *A&A*, 592, A18
- Masset F., 2000, *A&AS*, 141, 165
- Masson J., Chabrier G., Hennebelle P., Vaytet N., Commerçon B., 2016, *A&A*, 587, A32
- Masson J., Teyssier R., Mulet-Marquis C., Hennebelle P., Chabrier G., 2012, *ApJS*, 201, 24
- Matsumoto T., Machida M. N., Inutsuka S.-i., 2017, *ApJ*, 839, 69
- McKee C. F., Ostriker E. C., 2007, *ARA&A*, 45, 565
- McMullin J. P., Waters B., Schiebel D., Young W., Golap K., 2007, in Shaw R. A., Hill F., Bell D. J., eds, *Astronomical Data Analysis Software and Systems XVI Vol. 376 of Astronomical Society of the Pacific Conference Series, CASA Architecture and Applications*. p. 127
- Mercer A., Stamatellos D., 2016, *ArXiv e-prints*
- Meru F., 2015, *MNRAS*, 454, 2529
- Meru F., Bate M. R., 2011, *MNRAS*, 411, L1
- Meru F., Bate M. R., 2012, *MNRAS*, 427, 2022
- Meyer D. M.-A., Vorobyov E. I., Kuiper R., Kley W., 2017, *MNRAS*, 464, L90
- Mignone A., Bodo G., Massaglia S., Matsakos T., Tesileanu O., Zanni C., Ferrari A., 2007, *ApJS*, 170, 228
- Mignone A., Zanni C., Tzeferacos P., van Straalen B., Colella P., Bodo G., 2012, *ApJS*, 198, 7
- Mueller K. E., Shirley Y. L., Evans II N. J., Jacobson H. R., 2002, *ApJS*, 143, 469
- Myers A. T., Klein R. I., Krumholz M. R., McKee C. F., 2014, *MNRAS*, 439, 3420
- Myers A. T., McKee C. F., Cunningham A. J., Klein R. I., Krumholz M. R., 2013, *ApJ*, 766, 97
- Nelson R. P., Gressel O., Umurhan O. M., 2013, *MNRAS*, 435, 2610
- Ntormousi E., Hennebelle P., André P., Masson J., 2016, *A&A*, 589, A24
- Offner S. S. R., Klein R. I., McKee C. F., Krumholz M. R., 2009, *ApJ*, 703, 131
- Offner S. S. R., Kratter K. M., Matzner C. D., Krumholz M. R., Klein R. I., 2010, *ApJ*, 725, 1485
- Ormel C. W., Shi J.-M., Kuiper R., 2015, *MNRAS*, 447, 3512
- Paardekooper S.-J., 2012, *MNRAS*, 421, 3286
- Padoan P., Nordlund Å., 2011, *ApJ*, 730, 40
- Peters T., Banerjee R., Klessen R. S., Mac Low M.-M., Galván-Madrid R., Keto E. R., 2010, *ApJ*, 711, 1017
- Petrović J., 2004, PhD thesis, Utrecht University
- Pollack J. B., Hollenbach D., Beckwith S., Simonelli D. P., Roush T., Fong W., 1994, *ApJ*, 421, 615
- Pudritz R. E., Ouyed R., Fendt C., Brandenburg A., 2007, *Protostars and Planets V*, pp 277–294
- Purser S. J. D., Lumsden S. L., Hoare M. G., Urquhart J. S., Cunningham N., Purcell C. R., Brooks K. J., Garay G., Gúzman A. E., Voronkov M. A., 2016, *MNRAS*, 460, 1039
- Rafikov R. R., 2007, *ApJ*, 662, 642
- Rafikov R. R., 2009, *ApJ*, 704, 281
- Regály Z., Vorobyov E., 2017, *A&A*, 601, A24
- Reiter M., Kiminki M. M., Smith N., Bally J., 2017, *ArXiv e-prints*
- Rice W. K. M., Forgan D. H., Armitage P. J., 2012, *MNRAS*, 420, 1640
- Rice W. K. M., Lodato G., Armitage P. J., 2005, *MNRAS*, 364, L56
- Rice W. K. M., Paardekooper S.-J., Forgan D. H., Armitage P. J., 2014, *MNRAS*, 438, 1593
- Richling S., Yorke H. W., 1997, *A&A*, 327, 317
- Richling S., Yorke H. W., 1998, *A&A*, 340, 508
- Richling S., Yorke H. W., 2000, *ApJ*, 539, 258
- Rogers P. D., Wadsley J., 2012, *MNRAS*, 423, 1896
- Rosen A. L., Krumholz M. R., McKee C. F., Klein R. I., 2016, *MNRAS*, 463, 2553
- Rosen A. L., Krumholz M. R., Oishi J. S., Lee A. T., Klein R. I., 2017, *Journal of Computational Physics*, 330, 924
- Ruden S. P., Pollack J. B., 1991, *ApJ*, 375, 740
- Sakurai Y., Vorobyov E. I., Hosokawa T., Yoshida N., Omukai K., Yorke H. W., 2016, *MNRAS*, 459, 1137
- Sana H., de Mink S. E., de Koter A., Langer N., Evans C. J., Gieles M., Gosset E., Izzard R. G., Le Bouquin J.-B., Schneider F. R. N., 2012, *Science*, 337, 444
- Seifried D., Banerjee R., Klessen R. S., Duffin D., Pudritz R. E., 2011, *MNRAS*, 417, 1054
- Seifried D., Banerjee R., Pudritz R. E., Klessen R. S., 2012, *MNRAS*, 423, L40
- Seifried D., Banerjee R., Pudritz R. E., Klessen R. S., 2013, *MNRAS*, 432, 3320
- Seifried D., Banerjee R., Pudritz R. E., Klessen R. S., 2015, *MNRAS*, 446, 2776

- Seifried D., Pudritz R. E., Banerjee R., Duffin D., Klessen R. S., 2012, MNRAS, 422, 347
- Seifried D., Sánchez-Monge Á., Walch S., Banerjee R., 2016, MNRAS
- Shakura N. I., Sunyaev R. A., 1973, A&A, 24, 337
- Shu F. H., 1992, Journal of the British Astronomical Association, 102, 230
- Smith R. J., Hosokawa T., Omukai K., Glover S. C. O., Klessen R. S., 2012, MNRAS, 424, 457
- Stacy A., Greif T. H., Bromm V., 2010, MNRAS, 403, 45
- Stamatellos D., Whitworth A. P., 2009a, MNRAS, 392, 413
- Stamatellos D., Whitworth A. P., 2009b, MNRAS, 400, 1563
- Stepanovs D., Fendt C., Sheikhezami S., 2014, ApJ, 796, 29
- Stoll M. H. R., Kley W., 2014, A&A, 572, A77
- Takahashi S. Z., Tsukamoto Y., Inutsuka S., 2016, MNRAS, 458, 3597
- Tanaka K. E. I., Tan J. C., Staff J. E., Zhang Y., 2017, ArXiv e-prints
- Testi L., 2003, in De Buizer J. M., van der Blik N. S., eds, Galactic Star Formation Across the Stellar Mass Spectrum Vol. 287 of Astronomical Society of the Pacific Conference Series, Intermediate Mass Stars (Invited Review). pp 163–173
- Tomida K., Okuzumi S., Machida M. N., 2015, ApJ, 801, 117
- Tomida K., Tomisaka K., Matsumoto T., Ohsuga K., Machida M. N., Saigo K., 2010, ApJ, 714, L58
- Toomre A., 1963, ApJ, 138, 385
- Truelove J. K., Klein R. I., McKee C. F., Holliman II J. H., Howell L. H., Greenough J. A., Woods D. T., 1998, ApJ, 495, 821
- Tsukamoto Y., Takahashi S. Z., Machida M. N., Inutsuka S., 2015, MNRAS, 446, 1175
- Vaidya B., Fendt C., Beuther H., Porth O., 2011, ApJ, 742, 56
- van der Tak F. F. S., van Dishoeck E. F., Evans II N. J., Blake G. A., 2000, ApJ, 537, 283
- Vanbeveren D., 1991, Space Sci. Rev., 56, 249
- Vink J., 2012, A&A Rev., 20, 49
- Vink J. S., 2006, in Lamers H. J. G. L. M., Langer N., Nugis T., Annuk K., eds, Stellar Evolution at Low Metallicity: Mass Loss, Explosions, Cosmology Vol. 353 of Astronomical Society of the Pacific Conference Series, Massive star feedback – from the first stars to the present. p. 113
- Vorobyov E. I., 2010, ApJ, 723, 1294
- Vorobyov E. I., 2013, A&A, 552, A129
- Vorobyov E. I., 2016, A&A, 590, A115
- Vorobyov E. I., Baraffe I., Harries T., Chabrier G., 2013, A&A, 557, A35
- Vorobyov E. I., Basu S., 2007, MNRAS, 381, 1009
- Vorobyov E. I., Basu S., 2010, ApJ, 719, 1896
- Vorobyov E. I., Basu S., 2015, ApJ, 805, 115
- Vorobyov E. I., DeSouza A. L., Basu S., 2013, ApJ, 768, 131
- Woosley S. E., Heger A., Weaver T. A., 2002, Reviews of Modern Physics, 74, 1015
- Wurster J., Price D. J., Bate M. R., 2016, MNRAS, 457, 1037
- Yorke H. W., Sonnhalter C., 2002, ApJ, 569, 846
- Yorke H. W., Welz A., 1996, A&A, 315, 555
- Zapata L. A., Ho P. T. P., Schilke P., Rodríguez L. F., Menten K., Palau A., Garrod R. T., 2009, ApJ, 698, 1422
- Zhu Z., Hartmann L., Nelson R. P., Gammie C. F., 2012, ApJ, 746, 110
- Zinchenko I., Liu S.-Y., Su Y.-N., Salii S. V., Sobolev A. M., Zemlyanukha P., Beuther H., Ojha D. K., Samal M. R., Wang Y., 2015, ApJ, 810, 10
- Zinnecker H., Yorke H. W., 2007, ARA&A, 45, 481